UNIVERSITAT DE LES
ILLES BALEARS

Master Thesis

Dynamics of semiconductor lasers subjected to polarization rotated feedback and its application to fast random bit generation

Author:
Neus Oliver Andreu

Supervisors:
Ingo Fischer,
Miguel C. Soriano

March 15, 2012

The dissertation of Neus Oliver Andreu is approved:

Chair Date

Date

Date

University of Balearic Islands, The University of Balearic Islands

Winter 2012

Dynamics of semiconductor lasers subjected to polarization rotated feedback and its application to fast random bit generation

by

Neus Oliver Andreu

B.S.(Universitat de les Illes Balears) 2010

THESIS

Presented to

The University of Balearic Islands

in Partial Fulfillment

of the Requirements

for the Degree of

MASTER OF PHYSICS

March 2012

Dynamics of semiconductor lasers subjected to polarization rotated feedback and its application to fast random bit generation

Mit dem Wissen wächst der Zweifel.

Johann Wolfgang von Goethe.

Acknowledgements

Quiero agradecer en primer lugar a mis dos directores, Ingo Fischer y Miguel Cornelles, por su infinita paciencia y apoyo recibido desde el primer día. Las palabras de aliento de Ingo siempre consiguieron transformar mis frustraciones en motivaciones. Y las horas de aprendizaje en el laboratorio junto a Miguel hicieron que, poco a poco, me familiarizase con un entorno al que llegué sin saber nada. Mis agradecimientos también a David Sukow, a quien éste trabajo le debe mucho. Gracias a él, aprendí que en el laboratorio, ciencia y diversión pueden ir de la mano. Trabajar a su lado ha sido todo un honor. Tampoco quiero olvidarme de Claudio Mirasso, por sus contínuos ánimos, ni de Maxi San Miguel, por ofrecerme la posibilidad de unirme al IFISC.

A todos mis compañeros de doctorado. En especial a Ricardo, por sacarme siempre una sonrisa, aunque sea con sus barbaridades. A Luis, porque darse los buenos días es importante. A Juan, por estar siempre a mi lado. A Xavi, por aportar ese punto de humor a todas las conversaciones. A Konstantin, porque nunca le ha faltado tiempo para ayudarme. A Pablo, por las partidas de pádel que nos quedan. También quiero agradecer a Daniel Brunner, porque hablar con él supone aprender algo. A Marta, porque harta de estar siempre rodeada de hombres, el café con ella es más ameno. A Rosa, por escucharme y ser de confianza. Al "technical support": Antonia, Rubén, Edu y David. A pesar de las contínuas amenazas con bajarme la cuota, siempre han estado ahí cuando los he necesitado (y cada día puntualmente a las 10h).

Por último, gracias a mis padres, Guillermo y Juana, por hacer posible que hoy pueda escribir estas líneas y a mi hermano, mi "la". Finalmente, quiero dedicar esta tesis a Ángel. Por creer en mí mucho

más de lo que yo lo hago. Gracias por recordarme cada día que puedo. Gracias por estar ahí cada día.

Contents

1

Introduction and Motivation

In this Master Thesis we study the dynamics of semiconductor lasers subjected to delayed optical feedback, in particular, polarization rotated optical feedback (PROF). Optical feedback occurs when a fraction of the laser output is reinjected back into the laser cavity, normally due to the reflection of the light from a distant mirror. It has been observed that when a semiconductor laser is subjected to delayed optical feedback, the laser emission can be disturbed, exhibiting nonlinear dynamical behavior. These dynamics were contemplated as a nuisance that should be avoided, until it recently began to be considered as beneficial, taking advantage of the dynamical operation [1]. Nevertheless, a complete understanding of the delay dynamics is lacking. Many studies have been presented with lasers and optical feedback [2, 3, 4], but less attention has been given to feedback in which the polarization state of light is rotated. It was not until the early 1990s when thorough research and characterization of the dynamics of semiconductor lasers with PROF began [5]. Interest in this type of feedback has been increasing since then, prompting the emergence of new experimental work together with different mathematical models. Still, the studies so far have been inconclusive, as explained in Chapter 2, requiring a better description of the spectral and temporal features present in this system. This lack of experimental investigations with a complete characterization of the dynamical behavior motivated part of this thesis.

In addition, we believe that this characterization of the dynamics of semiconductor lasers under PROF, interesting in itself, was also necessary to understand the potential and increase the applicability of the system. In fact, the dynamical properties of the semiconductor laser subjected to PROF are significantly different from the dynamics of other optical feedback types, being specially favorable for chaotic applications. Within chaotic applications, one of current interest is the generation of sequences of random bits. Random bits play an important role in information security, complex numerical simulations, cryptography and gambling. Until recently, most of these demands were using the so called "pseudorandom generators" which are only deterministic algorithms utilized to generate the pseurandom bits. These pseudorandom generators have two fundamental problems. On the one hand, the

data generation speed is always limited by the speed of the electronic hardware. On the other hand, due to its deterministic nature, the unpredictability is bounded by the periodicity of the bit sequence. Consequently, the development of a system capable of generating true random bits was necessary. Many random bits generators have been presented up to today. Some are based on quantum mechanical uncertainty, being known as Quantum Random Bit Generators (QRBG) [6, 7] but their main disadvantage lies in the generation rate, which for the moment is in the order of Mbit/s while the modern data rates demand speeds three orders of magnitude faster. Other systems are laser-based, which generate random bits with different methods like using phase noise of the laser [9] or injecting light from a chaotic laser into a second laser [10]. The former has the same problem as the QRBGs, generating random bits at speeds up to 20Mbit/s. The latter, capable of generating bits at competitive rates, requires a system which enhances the bandwidth and where the polarization state is maintained along the entire setup, thus making it more expensive. To the best of our knowledge, this is the first work in which a single laser subjected to PROF is succesfully used to generate fast random bits.

For a better understanding of subsequent chapters, this introduction includes a brief summary of the main element on which this work is based, the semiconductor laser. We describe its operation and present the two types of semiconductor lasers most commonly used today, the so-called Edge-Emitting lasers (EELs) and Vertical Surface Emitting Lasers (VCSELs). We also report some differences between EELs and VCSELs in terms of emission and polarization properties. Finally, we end the introduction with an outline of this Ms Thesis.

1.1 Semiconductor lasers

Semiconductor lasers (SL) have turned into essential devices in just 40 years, not only in research, but also in our everyday lifes. Much of this is due to the enormous changes that lasers have undergone since their invention back in 1962 [11]. Today, a SL is much reduced in size, with low production cost and it is capable of converting current to coherent light in a highly efficient manner. Therefore, we can find SL in many applications which include, apart from telecommunications, holography, printing, welding, reading and recording discs, optical pumping of other lasers, material processing, medical, inter alia.

The word LASER is an acronym for Light Amplification by Stimulated Emission of Radiation, which describes how laser light is produced. Unlike the spontaneous emission process, where an electron in the conduction band relaxes to the valence band emitting a photon, the stimulated emission needs the presence of a photon in the medium, which causes the transition of an electron from the conduction band to the valence band with the subsequent emission of a new photon with the same propagation direction, wavelength and phase (coherent emission). Although there are many types of lasers today, all have certain elements in common which are

needed to achieve laser emission: a gain medium, a resonant cavity and a pumping system. These three elements are represented in Figure 1.1.

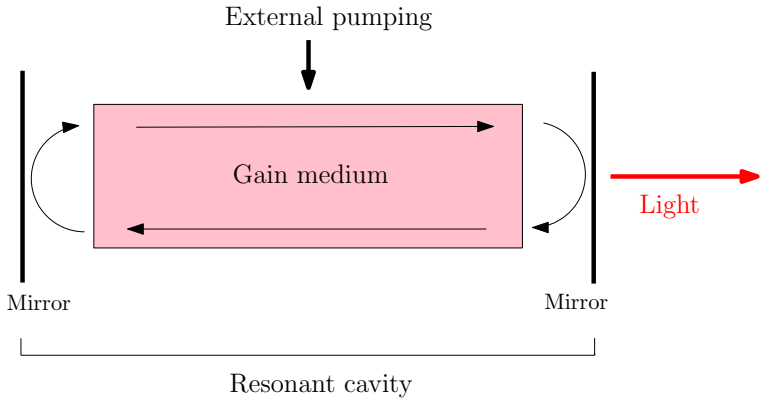

Figure 1.1: Illustration the laser cavity with its main elements.

In semiconductor lasers, the gain is achieved within a semiconductor p-n junction, into which an electric current is injected to achieve population inversion of electrons. A cavity, formed by a pair of mirrors, provides the selective feedback mechanism for the photons while traveling through the medium. In the process, a cascade effect takes place, stimulating the coherent emission of more photons. In the abscence of futher frequency selection mechanisms the emission frequency is governed by the longitudinal cavity mode whose frequency closely coincides with the gain peak frequency.

The device starts lasing only when the pump current exceeds the threshold value at which the gain compensates for all losses. These losses comprise mainly light scattering, light absorption and the transmission losses at the laser mirrors.

1.1.1 Types of semiconductor lasers

Semiconductor lasers are built with layers of semiconductor material grown on a substrate. The wafer is processed according to the geometry of the laser devices. SLs are grown mostly in two cavity geometries. On the one hand, there are the so-called Edge-Emitting semiconductor Lasers (EELs). The main feature of EELs is that light travels in the lateral plane inside an active layer where the recombination of electrons and holes takes place. The length of the resonant cavity can vary from 200 μm to a few milimeters, providing such a high gain that an EEL might even not need special reflecting coatings at the facets to lase. EELs are grown with Distributed Bragg Reflectors (DBR), as Distributed Feedback (DFB) lasers or using a Fabry-Perot cavity, which is a rectangular resonant cavity with cleaved facets at the ends of the cavity. In EELs, the laser beam is guided in a waveguide formed by a double heterostructure and lateral gain or index guiding. The double heterostructure confines the carriers to the active region, leading to a low threshold current. Figure

1.2 shows a schematic drawing of the typical structure of an Edge-Emitting Laser. The asymmetric lateral and transversal geometry of the emission area causes the beam from a typical EEL to be very divergent and astigmatic with an elliptic shape. The cross-section of the waveguide is typically a fraction of micrometers per several micrometers [12].

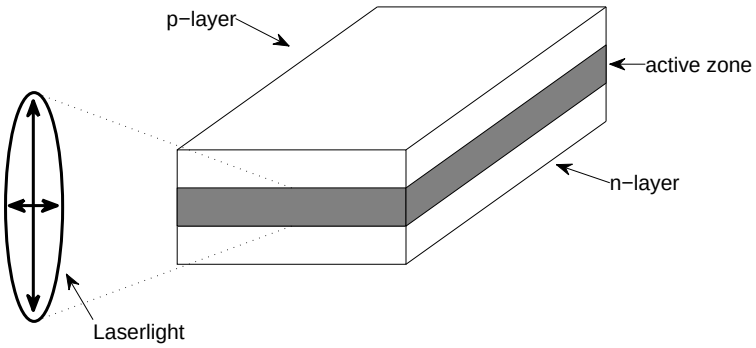

Figure 1.2: Illustration of the structure of an Edge-Emitting Laser.

More recently, devices designed to emit light in the direction perpendicular to the substrate appeared. These lasers are known as Vertical Surface Emitting Lasers (VCSELs) and were first proposed by Soda et al. [13]. In a VCSEL, the active layer is sandwiched between highly reflective mirrors, known as Distributed Bragg Reflectors (DBRs), composed of several dielectric layers. These mirrors must have a reflectivity of more than 99.5%, since the cavity of a VCSEL is shorter than for EELs and therefore the gain per round trip is smaller a priori. As a result, the light is emitted perpendicular to the layers from their top surface or the bottom of the device. The simple structural differences between VCSELs and EELs have important implications, but in our case, we will focus on the polarization differences. In Figure 1.3 we depict the structure of a VCSEL. The beam shape from a typical VCSEL is rather circular and larger than for an EEL, with a diameter that varies from 5 to 25 μm, so that the divergence is much lower and there are less astigmatism problems.

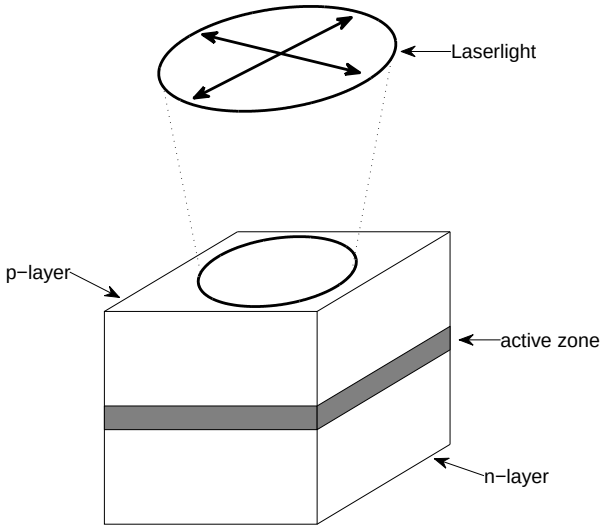

Figure 1.3: Illustration of the structure of a Vertical Cavity Surface Emitting Laser.

1.1.2 Polarization of laser light

Polarization is a property of electromagnetic waves that describes the vectorial orientation of the electric field. The polarization state of light can vary depending on the phase and amplitude of the orthogonal components of the electric field. When the perpendicular components are in phase and the electric vector oscillates in a constant direction, light is said to be linearly polarized. However, when the perpendicular components have the same amplitude and differ in phase by 90°, the electric vector appears moves in a circle, acquiring circular polarization. Another case is when the two components do not have the same amplitude or the phase offset is not 90°. This type of polarization is named elliptical polarization. The last case is when the direction of the polarization changes randomly and rapidly, then the light is said to be unpolarized, e. g. for spontaneous emission.

A coordinate system used for polarization directions is based on the plane of incidence, which is defined as the plane spanned by the propagation direction and a vector perpendicular to the reflecting surface. Transverse Electric (TE) polarized light is characterized by its electric field being perpendicular to the plane of incidence while the magnetic field lies in the plane of incidence. When the magnetic field is perpendicular to the plane of incidence, light is said to be Transverse Magnetic (TM) polarized. In such a case, the electric field lies in the plane of incidence.

The beam of an EELs is generally linearly polarized in two fixed directions: parallel to the heterojunction plane (TE polarization) or perpendicular to it (TM polarization). The two main mechanisms that cause the linearly polarized emission are the laser gain and the losses of the resonant cavity. Given the rectangular geometry of the EELs, the TM mode suffers greater losses at the facets, so that the emission is usually predominantly TE polarized in EELs.

In VCSELs, due to the cylindrical symmetry, all polarization directions experience similar gain and therefore there are no preferred directions a priori. This fact makes VCSELs more sensitive to polarization instabilities, choosing the orientation of the polarization due to imperfections or electro-optic and elasto-optic effects [14, 15]. Therefore, VCSELs generally emit linearly polarized light, that can switch to its orthogonal polarization orientation when some parameters, like the injection current, are changed. For transverse multimode VCSEL, both polarizations can contribute to the emission simultaneously.

1.2 Outline of this Ms Thesis

The aim of this Ms Thesis is to present an experimental analysis of an edge emitting semiconductor laser subjected to polarization rotated feedback and study its potential for the application of random bit generation. We started from the basic description of the semiconductor lasers and will end up with a laser-based random bit generator capable to generate random bit sequences at rates up to multi-Gbit/s.

To set a starting point, in this first chapter we presented an introduction to the semiconductor laser, describing some fundamental concepts as well as the differences in the structure and emission between the two main types of semiconductor lasers: Vertical Surface Emitting Lasers (VCSELs) and Edge-Emitting Lasers (EELs).

The second chapter presents the scheme of the experiment we have designed. We first present the emission characteristics of the edge-emitting laser used in this study. We develope the theory behind polarization-rotated optical feedback (PROF), introducing a new nomenclature that distinguishes the possibility that one or both modes are excited and contribute to the dynamics. The rate equation models developed so far are also presented, explaining their main advantages and limitations.

In the third chapter, we analyze in experiments the dynamical properties that occur when a laser is fed back with PROF. One of the main differences from the solitary laser is observed in the Power vs Injected current (PI) characteristics for TE and TM mode. The PI curve shows the output laser power as a function of the injected current and exhibits a threshold behavior characterized by the threshold current value, in which the stimulated emission starts to dominate over spontaneous emission. The PI characteristics for the TE mode presents a slight reduction of the threshold current when the laser is subjected to PROF, while in the case of TM mode, it goes from not being excited to be slightly excited. The rest of the properties are divided into spectral and temporal features. In both cases, the main parameters of change are the injected current and the feedback strength, studying their effects on power spectrum and autocorrelation function (AC). From the data obtained, we create a map of AC peak height for varying feedback and current conditions. This map presents a systematic study of the AC properties and it is a useful guidance for identifying the optimum conditions for a random number generator based on

chaotic laser dynamics.

Chapter 4 shows the applicability of the system presented, proving its effectiveness in the generation of random bits. In this chapter, we first present the digitization procedures, which include data acquisition with 8 bits analog to digital converters and bit truncation. We justify why their use is unavoidable, by plotting histograms and calculating the bias of the acquired bits. We also present the tool used to assess the randomness of the bit sequence: the NIST battery of randomness tests and provide a brief description of each of the tests. Finally, we present the results of these tests for an operating point within the optimal region defined by the AC map. We successfully generate random bits at a rate of 4Gbits/s with minimal postprocessing. The last section of this chapter includes a study of the role of postprocessing and dynamical conditions that allows to improve the bit rate up to 160 Gbit/s without any demanding postprocessing method.

The final chapter presents a summary of the main achievements presented in this Ms Thesis and a discussion of the future work demanded in this area.

2

Semiconductor Lasers with Polarization Rotated Optical Feedback: Experimental Setup and modeling

In this chapter we describe the effect of Polarization Rotated Optical Feedback (PROF) in the context of systems with delayed optical feedback. As the key element in this work, we first introduce some characteristic properties of the solitary Semiconductor Laser (SL) used in the experiments. Such properties are crucial to the dynamical behavior when the SL is subjected to delayed optical feedback. Our experimental setup, in which the polarization state of the light is rotated, is also explained. In the last section, we present the theoretical models for PROF, as well as a brief description of the results obtained so far in simulations and experiments.

2.1 Properties of the solitary laser

The laser used in our experiment is called Discrete Mode Laser manufactured by Eblana Photonics. This device is based on a Fabry-Perot (FP) cavity, with a waveguide structure that has been modified to obtain a single mode operation. This is achieved by etching features along the laser cavity, which causes a variation of the effective refractive index of the guided mode. A proper positioning of these etched structures allows the manipulation of the loss spectrum to have single mode emission with a very high side-mode suppression ratio. The threshold current of this laser is I_{th} =12.1 mA at 22°C.

Our Discrete Mode Laser presents asymmetric coatings to achieve high power emission from one laser facet, and low power emission from the other facet. The laser is fiber-pigtailed to the high power emission facet, which is produced with an anti reflection (AR) coating (less than 10% reflectivity), while the low power emission

facet is made with a high reflection (HR) coating (larger than 90% reflectivity). These asymmetric coatings lead to asymmetries of optical field and carrier density within the laser cavity. The influence of these asymmetric coatings in the presence of a laser subject to delayed optical feedback will be shown in Chapter 3.

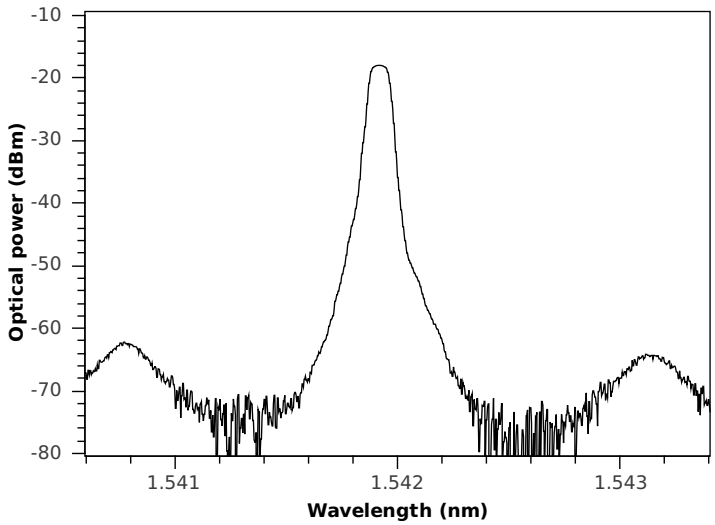

Figure 2.1: Experimental optical spectrum of the solitary laser at 15.50 mA.

In Figure 2.1 we depict an experimental optical spectrum of a Discrete Mode Laser at 15.50 mA and 22°C obtained directly from optical detection with an optical spectrum analyzer (Anritsu MS9710, 600-1750 nm wavelength range, 50 pm resolution). For these conditions, the measured wavelength is 1541.9 nm and the spectrum shows a narrow linewidth, which is below the resolution of the optical spectrum analyzer. The solitary laser displays a side-mode suppression ratio of more than 43 dB. The neighbouring modes correspond to non-lasing longitudinal cavity modes, which are spaced by 1.2 nm.

An important dynamical feature of SL are the relaxation oscillations, which are the result of the interaction between the carrier inversion and the optical field. The frequency of the relaxation oscillations characterizes this light-matter interaction in the laser medium and reflects the fast time scales present in the intensity dynamics of SL. These relaxation oscillations are decisive for the dynamical behavior of the SL since small perturbations, such as optical feedback, can undamp the oscillations. In figure 2.2 we show the optical spectrum with improved resolution obtained from a high resolution optical spectrum analyzer based on the Brillouin scattering effect (BOSA, Aragon Photonics,1528-1565 nm wavelength range, 0.08 pm resolution). The optical spectrum was measured at 19 mA and 22°C. We can observe a spectral profile with two small side maxima around 4 GHz. These resonances arise from the intensity and phase noise and their position coincides with the values ãão f the frequency of relaxation oscillations at each side of the laser peak emission.

Relaxation oscillation frequency can be more precisely identified from the elec-

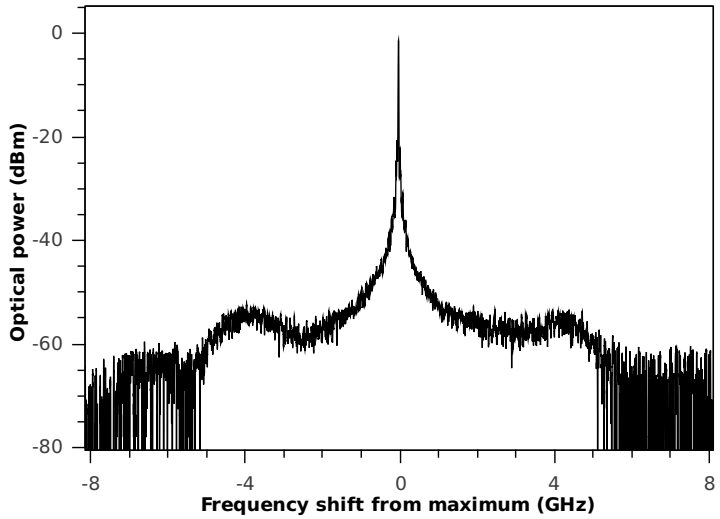

Figure 2.2. Optical spectrum of the laser at an injection current of 19 mA, corresponding to 1.57 I_{th}. The frequency shown is relative to maximum.

trical spectrum of the laser (Anritsu MS2667C, 9 kHz-30 GHz frequency resolution) after electrical conversion of the optical signal with a photodiode, as shown in figure 2.3 for 1.57 I_{th}. The relaxation oscillations frequency peak is observed to be around 4.3 GHz.

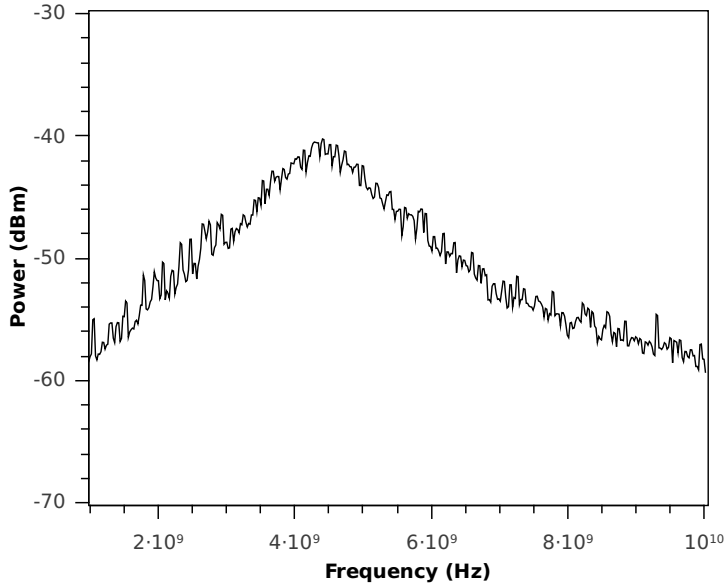

Figure 2.3: Experimental RF-spectrum of the laser pumped at 19 mA.

SL can exhibit relaxation oscillation frequencies of up to a few tens of GHz, depending on the type of SL used and the injection current. Telecommunication applications can benefit from this fast relaxation oscillations, which allow for a fast direct modulation of the lasers. The experimental results for the dynamical response

of this laser subject to PROF will be shown in Chapter 3.

2.2 Introduction to PROF

It is known that Semiconductor Lasers (SL) subject to delayed optical feedback exhibit a rich variety of complex dynamic phenomena. Most of the studies focused on systems with optical feedback which preserve the polarization state of the light in the feedback loop. In such cases, often an edge-emitting semiconductor laser is employed oscillating in single mode, commonly a transverse electric (TE) mode (see Chapter 1), and the light is reflected back into the cavity from an external mirror keeping a parallel polarization state. This type of delayed optical feedback has been typically named coherent feedback when the mirror or the reflecting element is placed within the coherence length of the laser. Lang and Kobayashi [16] presented in 1980 a rate equations model for these conditions and six years later, Tkach and Chraplyvy [17] exemplarily characterized the instabilities present in a 1.5-μm SL with coherent feedback defining 5 regimes depending on the feedback level. This coherent polarization mantained feedback is utilized in many applications including chaotic transmission, where it has been succesfully proven in high speed secure communications [40], chaotic Lidar [19] or even random number generation [20]. However, it is very difficult to guarantee a coherent feedback when light is transmitted in an optical fiber over a long distance.

Other schemes of delayed optical feedback have been studied recently, motivated by the practical benefits that systems which do not depend on a coherent polarization mantained feedback provide. When a laser is subjected to polarization-rotated optical feedback (PROF) the returned light has crossed polarization of the outgoing electric field. The polarization of the TE mode is rotated by 90° and the rotated beam is injected back into the laser cavity and vice versa. As a result, the intensity of TM mode is changed and acts on the TE mode through the carrier density giving raise to chaotic instabilities. This would be typically simulated by a rate equation model with two orthogonal linearly polarized electric fields [21]. This type of delayed optical feedback has been less studied in the literature and it has turned out to be a matter of confusion, as different experiments with mode polarization rotation led to different dynamics.

The term Incoherent Optical Feedback has often been used synonymously with PROF. For clarity, we prefer to make a clear distinction between them, considering that the effect is called incoherent when the PROF is small [22]. The word incoherent, despite of not being the best choice, is meant to refer that the delayed optical feedback does not directly contribute to the coherent field of the laser but only interacts with the carrier density. A numerical model which simulates this type of delayed feedback uses a single linearly polarized mode description and does not consider coherent interaction between two orthogonal fields [25].

Since both feedback types have their origin in the rotation of the polarization

state of the light, both are actual Polarization Rotated Optical Feedback cases. Moreover, the term *Incoherent Feedback* is too ambiguous, since it can have many interpretations. Not only can be referred to PROF, but it can also be understood as optical feedback in which the feedback loop exceeds the coherence length of the laser, or as a system subjected to electro-optical feedback. For these reasons, a new notation needs to be introduced. Based on the observed dynamics, we propose to call the first case presented as **PROF with 2 mode dynamics** and **PROF with single mode dynamics** for the incoherent optical feedback.

For the case of PROF with 2 mode dynamics, the majority of experiments and theoretical models focused on the situation where a single mode, usually the TE, was rotated and injected into the TM mode. This situation corresponds to a unidirectional coupling of polarization modes (TE $\rightarrow$ TM). However, there exists a more general scenario in which both polarization modes are rotated and injected into the corresponding orthogonal modes, leading to a bidirectional coupling between them (TE $\leftrightarrow$TM). Thus, PROF with 2 mode dynamics allows for two different coupling configurations between TE and TM modes (unidirectional and bidirectional), showing each a particular dynamical behavior.

Finally, a third case of optical feedback should be taken into account, where polarization is mixed and phenomena such as circular polarization or elliptical polarization are included [26]. The dynamical properties observed in the three general cases, polarization mantained, polarization rotated and mixed polarization optical feedback are quite different and not fully understood. In the following, we will focus on the implementation of systems subject to PROF, presenting our experimental configuration as well as the existing models to characterize it. A detailed discussion of the dynamics of PROF will be covered in Chapter 3.

2.3 The setup

For wide applicability (see Chapter 4), we have designed an experimental system that is simple, compact, robust, and made of relatively low-cost, standard, fiber-based telecom components. Optical feedback experiments have been typically implemented in free-space optics. Nevertheless, experiments aimed at telecommunication applications have been moved towards fiber-based setups, benefiting from their easy implementation and long distance transmission.

As illustrated in Fig. 2.4, the experiments involve a single semiconductor edge-emitting laser (Eblana Discrete Mode Laser), characterized in the previous section, with a wavelength of 1.54 μm and with a threshold current I_{th} = 12.1 mA at 22°C. The laser diode (LD) is fiber-pigtailed and connected to a 1x2 90/10 optical coupler (OC) the principal output of which passes through a variable optical attenuator (ATT) used for feedback strength control. A Faraday mirror (FM) is the source of PROF and its behavior is based on the Faraday Effect.

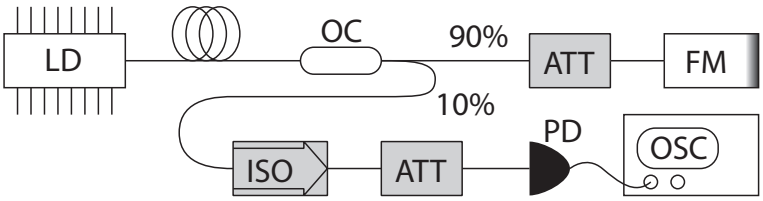

Figure 2.4: Experimental schematic diagram. Definitions can be found in text.

The Faraday effect, illustrated in Fig. 2.5, describes the rotation of the polarization of a signal, as it passes through certain optical media within a magnetic field. Located at the end of the optical fiber, the Faraday mirror is designed to rotate the polarization state by 45°, twice once when the light enters, and again when the light is reflected back into the fiber. Since the Faraday effect is non-reciprocal, the resultant polarization of light is rotated by 90° with respect to the original signal and injected back into the laser.

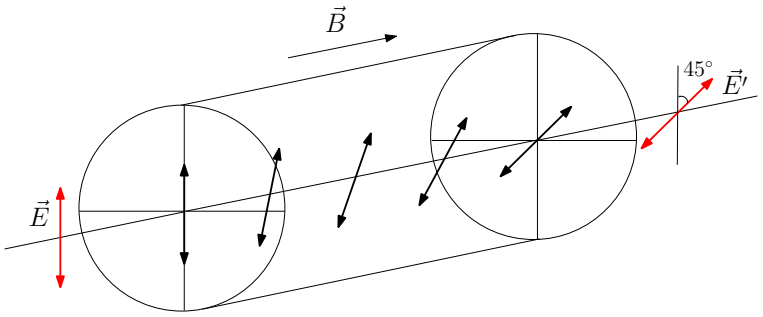

Figure 2.5: Illustration of the Faraday effect.

Our practical implementation of the external cavity has a roundtrip delay time of $\tau = 90.9$ ns and the light reinjected in the cavity is estimated to be up to 10-20% of the emitted output intensity. In this experimental setup, any polarization mode dispersion or birefringence that occur anywhere along the optical fiber is exactly compensated for. Moreover, this configuration can produce strong feedback, which will prove to be an important element in our study.

The light exiting the 10% port of the optical coupler is used for detection. It passes through an inline optical isolator (ISO) and is detected by a fiber-coupled photodetector (PD, Miteq 12.5 GHz bandwidth). The signal is captured by a digitizing oscilloscope (LeCroy 816Zi, 16 GHz analog bandwidth, 40 GS/s sample rate, 8-bit ADC).

2.4 The PROF models

In this section we present the existing rate equations models for polarization rotated optical feedback together with the most representative dynamical features the

models reproduce. In the first part a model describing the situation of PROF with 2-mode dynamics is introduced, whereas in the second part we show different models for PROF in which the dynamics is determined by a single mode.

2.4.1 PROF with 2-mode dynamics

One of the first models that accounted for 2-mode dynamics was proposed for polarization self-modulation in vertical-cavity surface-emitting lasers (VCSELs) [38]. VCSELs usually have two orthogonal linearly polarized mode emission which either coexist or one polarization mode dominates. When a mirror and a quarter-wave plate with its principal axes oriented at 45° with respect to the TE and TM directions are placed in the setup, the intensity dynamics of the laser is found experimentally to go through a polarization switching with a square-wave shape. The numerical model for the two polarization modes adds to the amplitudes and phases of the electric field a delayed term, accounting for the feedback from the external mirror. The complete set of dimensionless rate equations is given by (the subscripts indicate the TE and TM modes):

$$\frac{dE_{TE}(t)}{dt} = \frac{1}{2}[(2N+1)G_{TE} - 1]E_{TE} + \eta E_{TM}(t-\tau)cos(\psi_{TE}) \tag{2.1}$$

$$\frac{d\phi_{TE}(t)}{dt} = \Delta + \alpha N + \eta E_{TM}(t-\tau)sin(\psi_{TE}) \tag{2.2}$$

$$\frac{dE_{TM}(t)}{dt} = \frac{1}{2}[(2N+1)G_{TM} - 1]E_{TM} + \eta E_{TE}(t-\tau)cos(\psi_{TM}) \tag{2.3}$$

$$\frac{d\phi_{TM}(t)}{dt} = \alpha N + \eta E_{TE}(t-\tau)sin(\psi_{TM}) \tag{2.4}$$

$$T\frac{dN(t)}{dt} = J - N - (1+2N)[G_{TE}|E_{TE}|^2 + G_{TM}|E_{TM}|^2] \tag{2.5}$$

In these equations, E and ϕ are the amplitude and the phase of the electric field and N is the carrier density. Time is measured in units of the photon lifetime τ_p, α is the linewidth enhancement factor and Δ is the frequency detuning. The feedback strength is denoted by η. T is the ratio of the carrier lifetime to the photon lifetime and τ is the delay time. J denotes the pumping above threshold and the terms ψ_{TE} and ψ_{TM} are the phase differences. Nonlinear gain saturation is included via the factors G_{TE} and G_{TM}, which are described by:

$$G_{TE} = 1 - \kappa_{TE}(E_{TE}^2 - P/2) - \kappa'_{TE}(E_{TM}^2 - P/2) \tag{2.6}$$

$$G_{TM} = 1 - \kappa'_{TM}(E_{TE}^2 - P/2) - \kappa_{TM}(E_{TM}^2 - P/2) \tag{2.7}$$

κ_{TE} and κ_{TM} are the self saturation coefficients and κ'_{TE} and κ'_{TM} are the cross saturation coefficients. The term P/2 represents the approximate steady state intensity of each mode. With these rate equations their experimental results are reproduced qualitatively. Single mode emission is achieved in a wide parameter

regime, although stable TE and TM mode polarization switching can be found depending on the feedback strength and cavity length. Polarization self-modulation is obtained for frequencies up to 9.18 GHz. More recently, a paper by Sukow et al. [24] showed that square-waves of polarization switching also appear in the intensity dynamics of two edge-emitting lasers mutually coupled with polarization rotated injection.

An alternative model which had a high impact was the one presented by Heil et al. [21], motivated by the contradictions found between their experimental results and previous theoretical works. In their two-mode dynamical model the emission of the TE mode is injected with delay into the TM mode of the laser. Therefore, the amplitudes and phases of the TE and TM-modes are time dependent functions. The rate equations for the TE and TM modes are described as follows:

$$\frac{dE_{TE}(t)}{dt} = \frac{1}{2}\{G_{TE}[N(t) - N_0] - \gamma_{p,TE}\}E_{TE}(t) \tag{2.8}$$

$$\frac{d\phi_{TE}(t)}{dt} = \frac{1}{2}\alpha\{G_{TE}[N(t) - N_0] - \gamma_{p,TE}\} \tag{2.9}$$

$$\frac{dE_{TM}(t)}{dt} = \frac{1}{2}\{G_{TM}[N(t) - N_0] - \gamma_{p,TM}\}E_{TM}(t) + \gamma_{inj}E_{TE}(t-\tau)cos\Delta(t) \tag{2.10}$$

$$\frac{d\phi_{TM}(t)}{dt} = \frac{1}{2}\alpha\{G_{TM}[N(t) - N_0] - \gamma_{p,TM}\} - \gamma_{inj}\frac{E_{TE}(t-\tau)}{E_{TM}(t)}sin\Delta(t) \tag{2.11}$$

$$\frac{dN(t)}{dt} = J - \gamma_s N(t) - [N(t) - N_0]\{G_{TE}|E_{TE}(t)|^2 + G_{TM}|E_{TM}(t)|^2\} \tag{2.12}$$

$$\Delta(t) = \omega_0\tau + \phi_{TM}(t) - \phi_{TM}(t-\tau) \tag{2.13}$$

Where E and ϕ are the amplitude and the phase of the electric field. N is the carrier density and Δ is the phase difference. $G_{TE,TM}$ are the gain coefficients and N_0 is the carrier density at transparency. γ_p is the inverse of the photon lifetime, γ_{inj} is the injection coefficient and γ_s is the inverse of the carrier lifetime. The delay time of the external loop is denoted by τ, α is the linewidth enhancement factor, J is the current density and ω_0 is the angular frequency. Due to a polarizer placed in the experimental setup, TM mode is not allowed to be coupled back to the TE mode.

These equations reproduce their experimental findings, where the slope of the PI curve remains unchanged for the total output power. This model also describes general features of the dynamics subjected to PROF which depend on the feedback strength and injection current. The dynamics they observe is weakly chaotic with instabilities of small amplitude. Strong feedback is required for the origin of the instabilites and strong pumping is needed for their extinction. Moreover, the peaks appearing in the RF-spectrum, associated to the round-trip frequency, remain constant in position.

2.4.2 PROF with single mode dynamics

The most widely accepted model for PROF with single mode dynamics was first proposed by Otsuka and Chern [25] back in 1991. In this situation, the reflected beam is orthogonal to the emitted laser field. The reflected laser beam does not interfere with the coherent field, but it interacts with the carrier density. This effect can be written in the equations by adding a delayed optical feedback into the carrier-rate equation, coupling the two differential equations. The model is described by the following rate equations:

$$\frac{dS(t)}{dt} = \{G_n[n(t) - n_0]\}S(t) \tag{2.14}$$

$$\frac{dn(t)}{dt} = \frac{J}{ed} - \frac{n(t)}{\tau_s} - \{G_n[n(t) - n_0]\}[S(t) + \kappa' S(t - \tau)] \tag{2.15}$$

where S and n are the photon density and the population-inversion density, respectively. Moreover, κ' is the feedback coefficient,τ_s is the carrier lifetime and τ again the delay time. The model results in sustained pulsations in the output of the laser, which can be chaotic or regular. The repetition rate of these pulses is determined by relaxation oscillations. A more detailed experimental study was conducted by Houlihan et al. [27], who determined that instabilities appear in the dynamics due either to enhancement of the mode partition noise or relaxation oscillation and roundtrip time of the external cavity.

In 2005 Ju et al. [28] proposed a similar model of coupled differential equations for incoherent feedback:

$$\frac{dS(t)}{dt} = \{\Gamma G_n[N(t) - N_0] - \frac{1}{\tau_p}\}S(t) + R_{sp} \tag{2.16}$$

$$\frac{dN(t)}{dt} = \frac{I}{eV} - \frac{N(t)}{\tau_s} - \{G_n[n(t) - n_0]\}S(t) - \kappa\gamma\{G_n[n(t) - n_0]\}S(t - \tau) \tag{2.17}$$

In this case, Γ is the confinement factor,τ_p is the photon lifetime, R_{sp} indicates the spontaneous emission, I is the bias current and V denotes the volume of the active region. γ is the ratio of the TM and TE gain and κ is the coupling factor, which they derived it to be:

$$\kappa = [(1 - r_2^2)\frac{r_3}{r_2}]^2 \tag{2.18}$$

where r_1 and r_2 denote the reflectivities of the facet of the laser and r_3 the external reflectivity. Assuming that TE and TM gains are the same, this model reproduces a threshold reduction in the PI curve, although this reduction is not as significant as in the coherent polarization mantained feedback case. The model also describes four dynamical regimes depending on the feedback level: stable, chaotic, pulsed and two-state regime. For the pulsed regime, the injection current plays an important role, controlling the pulse repetition frequency, pulsewidth and pulse power. With

their simulations and experiments they also conclude that under no circumstance the TM mode contributed to lasing [29].

Based on the equations of Otsuka and Chern another model was proposed in 2003 by Cheng et al. [30]. It presented some corrections to the original model, where the TE and TM waves are considered again separately:

$$\frac{dN(t)}{dt} = \frac{I}{e} - \frac{N(t) - N_0}{\tau_e} - v_g\{G_E S_E(t) + G_M[S_M(t) + \gamma S_E(t-\tau)]\} \tag{2.19}$$

$$\frac{dS_E(t)}{dt} = \Gamma_E v_g G_E S_E(t) - \frac{S_E(t)}{\tau_{pE}} + R_{sp} \tag{2.20}$$

$$\frac{dS_M(t)}{dt} = \Gamma_M v_g G_M[S_M(t) + \gamma S_E(t-\tau)] - \frac{S_E(t)}{\tau_{pM}} + R_{sp} \tag{2.21}$$

in which the gains of the TE and TM mode are described by:

$$G_E = A_E[N(t) - N_0] - [\kappa_E S_E(t) + \kappa'_E S_M(t)] \tag{2.22}$$

$$G_M = A_M[N(t) - N_0] - [\kappa'_M S_E(t) + \kappa_M S_M(t)] \tag{2.23}$$

S_E and S_M are the photon number of the TE and TM mode respectively. v_g is the group velocity and Γ_E and Γ_M are the confinement factor of the TE and TM mode. κ_E and κ'_E are the self-saturation and cross-saturation coefficient of TE mode, while κ_M and κ'_M represent the self-saturation and cross-saturation coefficient of TM mode.

These equations, which assume TE and TM modes to be lasing simultaneously, allow for an independent gain for each mode, thus improving the capabilities of the model and obtaining more realistic feedback ratios. Therefore, despite being based on a originally unimodal model, it represents an option to characterize the dynamics of two modes with PROF. However, it is not rigorously justified why the feedback term is accounted for in both the equation for $N(t)$ and $S(t)$.

Determining which of these models is the most appropiate one for certain conditions is a difficult task. So far, the criteria used to choose one instead of another has been based on the experimental results, selecting the model which more accurately reproduces the real behavior of the system. The current models have been divided into two branches, one that represents the dynamics of the system based on a description of the electric field for the TE and TM modes (PROF with 2-mode dynamics), and another in which there is no coherent interaction between the orthogonal components of the electric field (PROF with single mode dynamics). Future models should consider not only the TE to TM mode injection, but also the case where TM is injected to TE mode and see how these polarization mode rotations, after one delay time, interact with the optical field.

3

Dynamical properties of semiconductor lasers subject to Polarization Rotated Optical Feedback

The emission properties of semiconductor lasers are altered when subjected to delayed optical feedback. In fact, semiconductor lasers are especially sensitive to feedback light, exhibiting a destabilized power output. These instabilities present in the laser emission were long considered a detriment and optical isolators were used to avoid any incoming reflection. It was a good decade ago when a new point of view was adopted. Feedback-induced instabilities, result of the strong nonlinearities, can lead to a high-dimensional chaotic dynamics, which has also been recognized to have attractive properties for photonic applications. For instance, broadband chaotic dynamics of semiconductor lasers can be used for encrypted communication [33, 34], chaotic lidars [19], rainbow refractometry [35], random bit generation [20] or eventually information processing.

This chapter discusses the main dynamical properties characteristic for the laser subject to polarization rotated optical feedback (PROF). In the first section of the chapter we discuss the changes present in the power vs injected current (PI) characteristic of a laser with PROF. This dependency characterizes the amount of light emitted as a function of the injected current in to the laser. The current at which the laser starts to lase is typically referred to as threshold current. In this chapter, spectral and temporal features are also introduced. The electrical spectrum of the laser and the autocorrelation function are also modified due to PROF. These changes are studied in terms of the injected current and the feedback strength. Finally, we develop a map with the most relevant information on the temporal dynamics of a SL subject to PROF. This map will be very useful for the intended application: random bit generation. How this application is carried out will be explained in Chapter 4.

3.1 Polarization resolved PI curves

We first measure the PI characteristic providing the output power as a function of the injection current. The PI characteristic shows the threshold behavior, above which the laser power increases linearly with increasing injection current. For our Eblana laser, this threshold current is 12.1 mA. One of the typical features of the parallel polarization mantained feedback is the threshold reduction of the injection current. The threshold reduction can be up to 20% depending on the feedback strength [31]. This is due to reduction of cavity losses caused by the photons re-injected into the laser cavity. Moreover, a pronounced kink appears close to the solitary laser threshold, as a result of the low frequency fluctuations of the light intensity. The slope of the PI curve is also altered when the laser is subjected to polarization mantained delayed feedback, being affected due to the change in the external differential quantum efficiency and the change in balance of the effective output facet reflectivity.

In the case of polarization rotated feedback no threshold reduction would be expected, if the re-injected light interacted only with the carrier density [27]. However, experiments conducted so far are not decisive on this matter. While some authors state that with polarization rotated feedback there is no threshold reduction and the slope efficiency remains the same [21], others observed a different behavior: a small threshold reduction and a reduced slope efficiency [28]. Houlihan et. al [27] observed no change in the laser threshold and a monotonic decrease in the slope efficiency when increasing the feedback level. Interestingly, they observed a slope reduction of 50% when around 70% of the total light was re-injected. A study investigating three different feedback configurations experimentally [29], showed that a small threshold reduction was present in the polarization rotated optical feedback.

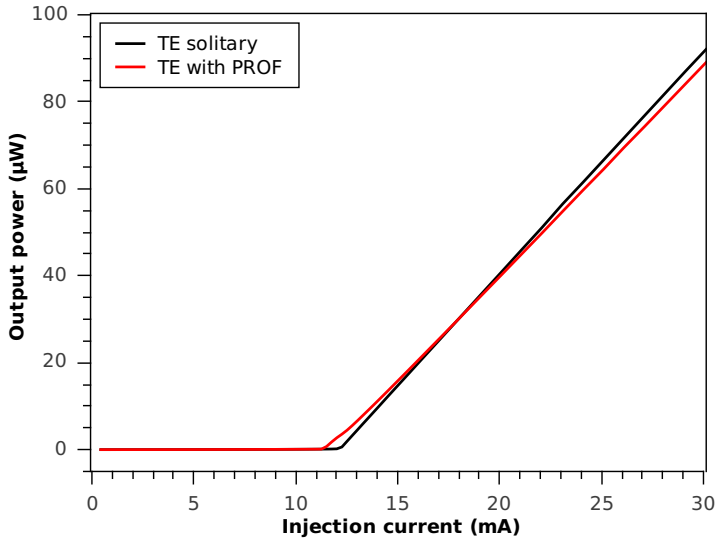

Figure 3.1: TE resolved PI curves for the solitary laser and for the laser with PROF.

In Figure 3.1 we present the measured PI characteristic for the TE mode of the solitary laser (black line) and the laser with polarization rotated feedback (red line). With rotated feedback, the TE mode has two differences compared with the solitary laser: the threshold is 8% decreased and the slope above threshold is smaller.

The PI characteristic for the TM mode of the solitary laser (black line) and the laser with polarization rotated feedback (red line) is shown in Figure 3.2. We can make sure to have rotated feedback effects, as evidenced by the growth of TM power for the PROF case, while in the solitary laser case the TM mode is not lasing. One should note that, although TM mode is excited with PROF, the TM output power is much smaller (around 96%) than the TE mode power.

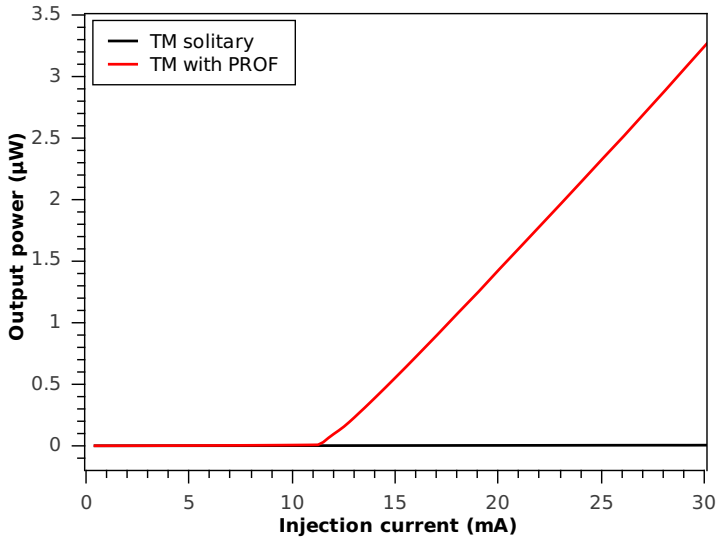

Figure 3.2: TM resolved PI curves for the solitary laser and for the laser with PROF.

3.2 Spectral features

RF-spectra are also useful indicators of the changes that occur when the laser is subjected to PROF. Figure 3.3 depicts two RF-spectra corresponding to the laser diode with and without PROF and taken at the same injection current (19 mA). For a better comparison, the vertical scale of the laser with PROF spectrum has been placed at the right axis. The solitary laser spectrum presents a clear peak at 4.3 GHz, introduced in Chapter 2 as the relaxation oscillations frequency peak. However, the main feature is the broadening of the RF-spectrum, originated from the chaotic changes in the intensity of the emitted light. A broad power spectrum is considered to be a necessary feature to produce randomness, since it mimics real noise.

All the spectra present in this chapter (except Figure 3.3 and Figure 3.5)

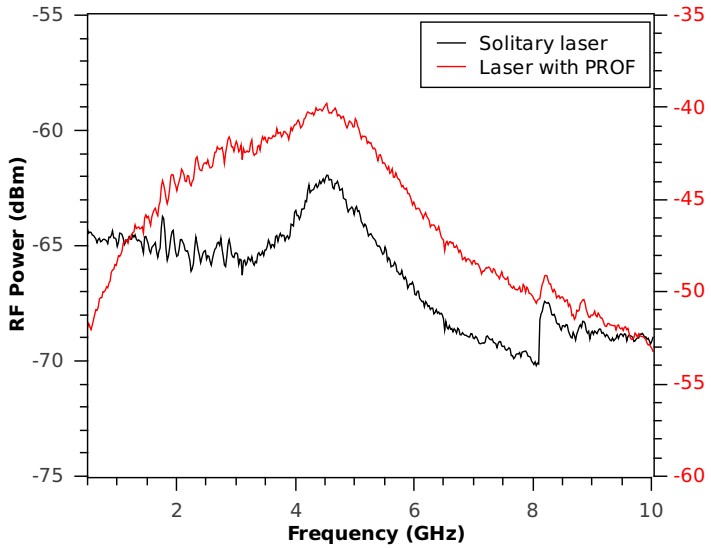

Figure 3.3. Experimental optical spectra of the solitary laser and the laser with PROF at 19 mA.

were taken without averaging, and with the same resolution bandwidth of 3 MHz. Indeed, the obtainable smooth broadband spectra are an advantage of our chosen configuration. For short cavities with delay times of order 0.5 ns, comparably smooth spectra have been obtained for polarization mantained feedback [35]. For longer cavities, however, with their higher dimensional dynamics, these properties have been achieved only with strong polarization-rotated feedback. It is quite unusual for delayed feedback lasers to show no structure relating to the roundtrip and no pronounced relaxation oscillations frequency in the power spectra. We can state that, in addition to their importance for our application, these broad spectra are interesting in their own right and merit further study.

Figure 3.4 shows power spectra at different pump currents I and feedback strengths, acquired with an RF spectrum analyzer (Anritsu MS2667C). In this case, feedback strength is quantified as the fractional power transmission T in the external cavity, that is, the ratio of power reentering and emerging from the laser pigtail. This is a convenient operational definition, although it does not include laser to fiber coupling efficiency. Figures 3.4(a) and 3.4(b) are for equal, strong feedback (T=52.2%) but different currents: 14.1 mA and 18.3 mA, respectively. Both display broad spectra with no evident dominant frequencies. The same features are noticeable in figures 3.4(c) and 3.4(d), obtained for equal, moderate feedback strength (T=33.7%) but for different currents: I=14.1 mA (3.5(c)) and I=18.3 mA (3.4(d)). In contrast, the spectra of Fig. 3.4(e) and Fig. 3.4(f) are for the same currents as plots (c) and (d), but for lower feedback (T=16.9%). Plot (e) shows a clear frequency peak (relaxation oscillation peak), while plot (f) displays greater structure with two evident peaks (relaxation oscillation peak and its second harmonic), and therefore would be considered less suitable for randomness applications.

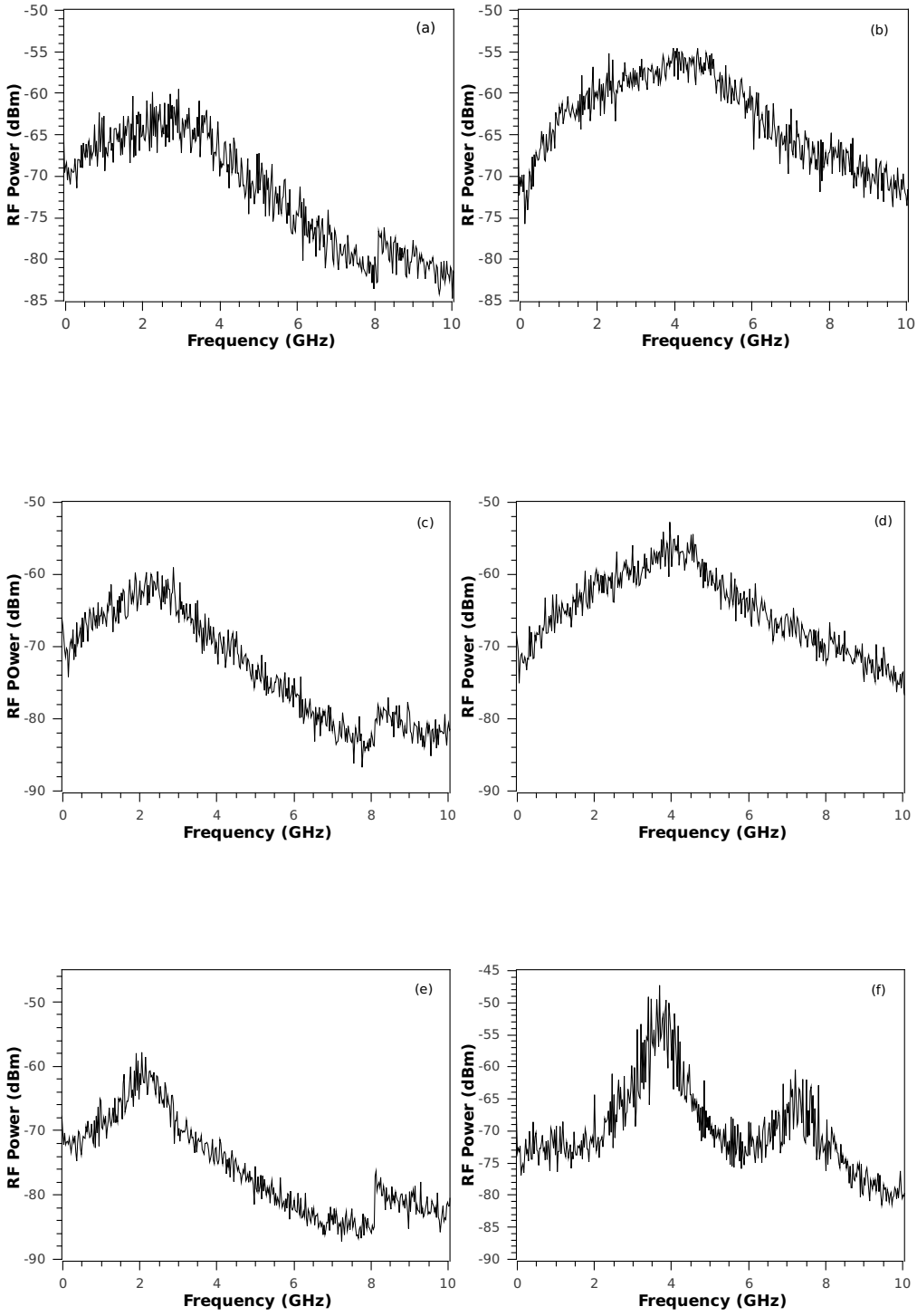

Figure 3.4. Power spectra of the laser intensity for a) I=14.1mA and T=52.2%; b)I=18.3mA and T=52.2%; c)I=14.1mA and T=33.7%; d)I=18.3mA and T=33.7%; e)I=14.1mA and T=16.9%; e)I=18.3mA and T=16.9%.

In the conditions similar to Fig. 3.4 (b), the signature of the external cavity

modes can be identified with a magnification of the RF spectrum, as depicted in Fig. 3.5. The spacing corresponds to the external cavity roundtrip frequencies. The observed mode spacing is $\Delta f \sim 5.4$ MHz. This corresponds to twice the roundtrip time (2τ), meaning that alternating modes are separated by one delay time ($\tau \sim 91.5$ ns). The mode spacing can be translated into a cavity length of L ~ 8.2 m.

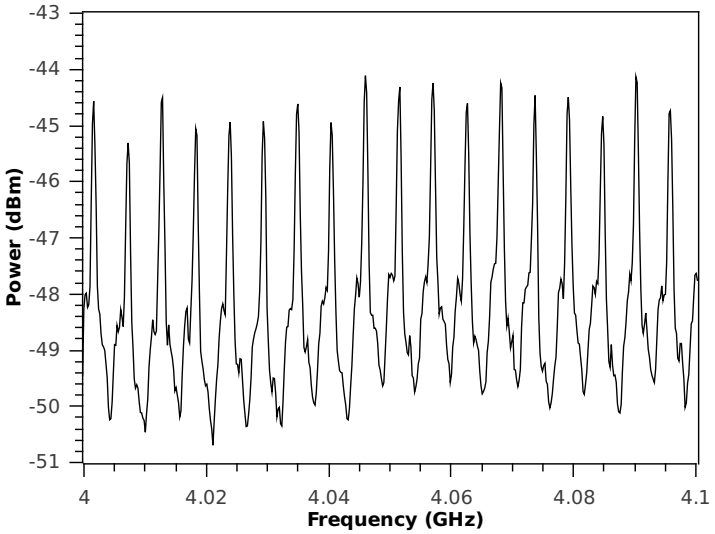

Figure 3.5. RF-spectrum of a SL with PROF showing the external cavity modes. The pump current is 19 mA.

Very recent studies on PROF systems have involved low or moderate feedback, where spectral structures are more apparent but the strong-feedback chaotic case has not been studied thoroughly. The ability to access this regime experimentally is critical for our random bit generation study, presented in Chapter 4, and full characterization of these interesting dynamics is a related topic of ongoing research.

3.3 Temporal features

One main feature of a laser subject to delayed optical feedback is the destabilization of the output intensity. This causes unstable dynamics with unpredictable changes in the amplitude of the signal. Figure 3.6 depicts a zoom into a time trace. The fluctuations are in the sub-nanosecond scale. Therefore, they could not be easily resolved until the appearance of fast photodetectors and oscilloscopes with high bandwidth.

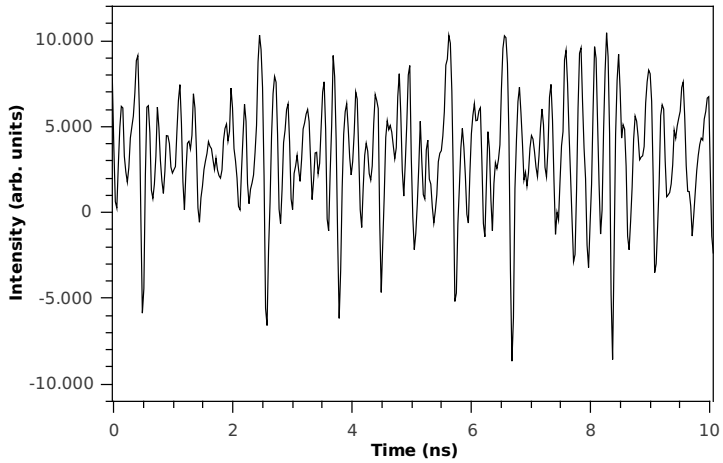

Figure 3.6: Chaotic oscillations in the output intensity of a SL pumped at $1.52I_{th}$ with PROF.

The external cavity roundtrip frequencies at integer multiples of $1/\tau$ are also evident in the time domain. The corresponding timescale τ appears in autocorrelation (AC) functions of time traces. The autocorrelation function between times t and s is defined as:

$$AC(s) = \frac{< [x(t) - < x(t) >][x(t-s) - < x(t) >] >}{< [x(t) - < x(t) >]^2 >} \tag{3.1}$$

Fig. 3.7. shows the data of the AC function up to a time shift of 1000 ns and corresponds to the same operating conditions as Fig. 3.6. Figures 3.7 (a) and 3.7 (b) were obtained under the same feedback level (T=52.2%) but different pumping current (14.1 mA and 18.3 mA respectively). Similarly, Figures (c) and (d) were acquired for the same injection currents but a power transmission of 33.7%. No significant changes can be observed between plots 3.7 (a), (b), (c) and (d). Peaks in the AC function appear at integral multiples of τ=91.5 ns, as is typical for delayed feedback systems. However, the 2τ peak of the AC function is always the largest. For plot 3.7 (b), the height of the AC peak at the first odd multiple of the delay time is 0.02, which makes it almost imperceptible, while the first even multiple is 0.18. This is a particular characteristic of the PROF systems, due to the rotation of the polarization state of the light. The polarization of the travelling light is parallel to the original emitted light of the laser after two roundtrips, causing a major contribution to the even-multiple AC peaks.

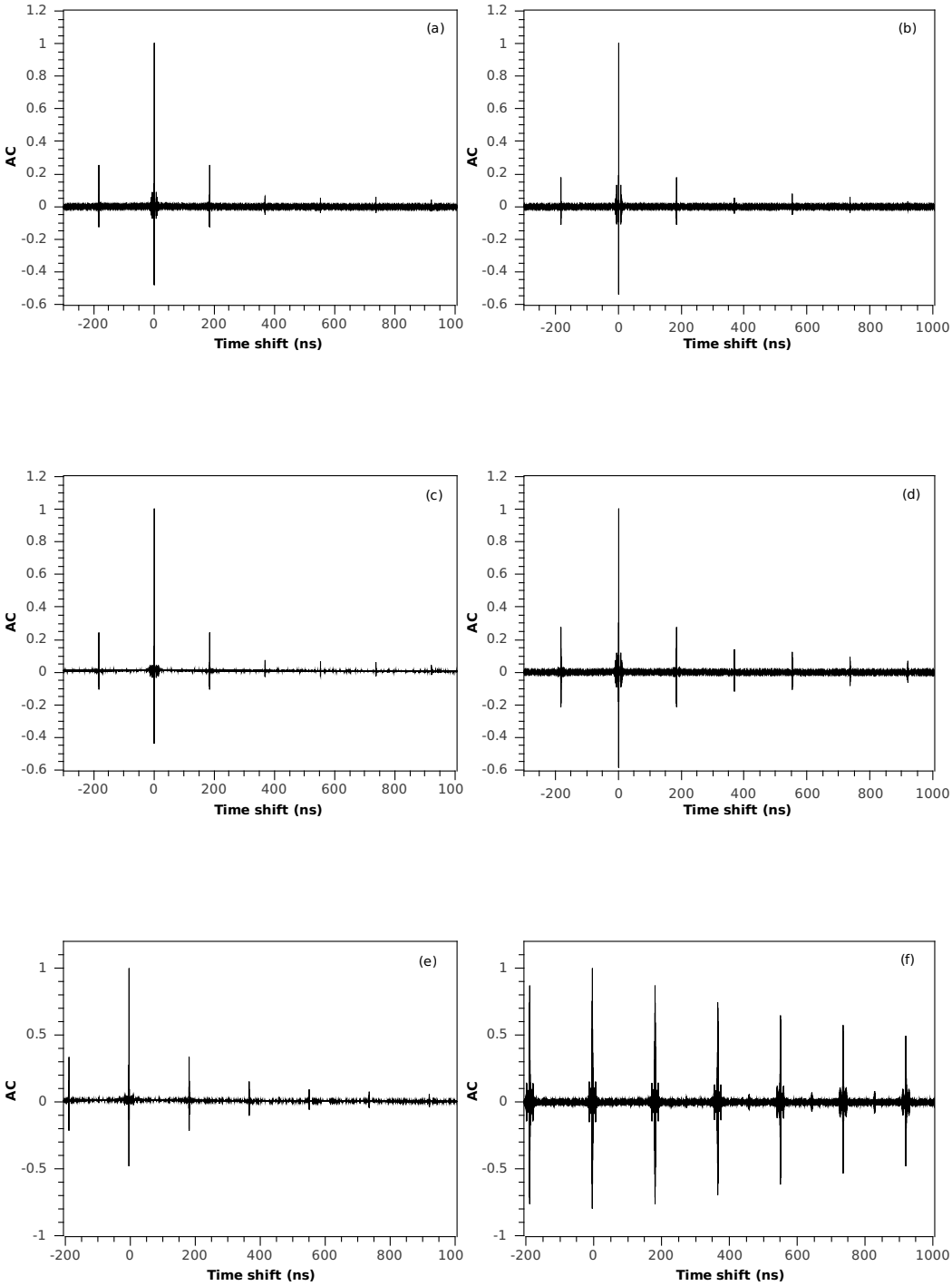

Figure 3.7. Autocorrelation function of the intensity dynamics for a) I=14.1mA and T=52.2%; b)I=18.3mA and T=52.2%; c)I=14.1mA and T=33.7%; d)I=18.3mA and T=33.7%; e)I=14.1mA and T=16.9%; f)I=18.3mA and T=16.9%.

Other features of interest can be seen from Figures 3.7 (e) and (f). Keeping the feedback level constant at 16.9%, the autocorrelation function exhibits drastic

changes in the height of the AC peaks when increasing the pumping current from 14.1 mA (Fig. 3.7(e)) to 18.3 mA (Fig. 3.7(f)). In the latter plot, the first even multiple of τ is around 0.9, having a correlation almost as high as for the zeroth peak.

Figure 3.8 shows a detail of the autocorrelation function of the intensity dynamics obtained for I=18.3 mA and a power transmission of T=52.2 %, describing the same conditions as Figure 3.7 (b). The resolved AC function around zero time shift, is depicted in Fig. 3.8 (a) which decays rapidly. In particular, correlations between points in time are lost within 1 ns. For completeness, Figure 3.8 (b) shows the AC function around the second AC peak, typically larger than the first. The structure of the second peak is smaller compared to the zeroth peak, slightly asymmetric, and also presents a faster decay. The AC peak heights at multiples of τ and the width of the zeroth peak both provide useful criteria for tailoring the dynamics. Minimizing the height of a delay time peak selects operating conditions for the laser system at which temporal correlations in the intensity are weakest. In contrast, choosing a random sample interval that is longer than the AC decay time helps assure that successive points will be independent of one another.

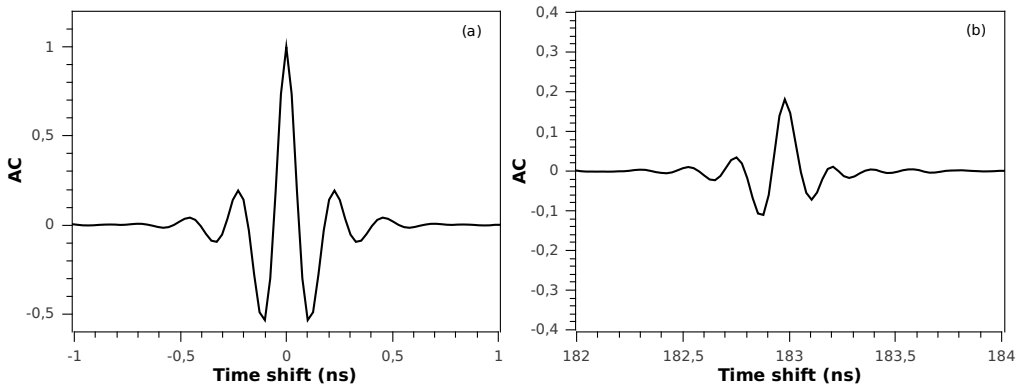

Figure 3.8. AC function of the intensity dynamics: a) For the resolved zeroth AC peak; b) For the resolved second AC peak.

3.4 Systematic study of the AC properties and discussion

For a systematic study of the autocorrelation properties, we examine the height of the AC peak at time shifts of 2τ as a function of laser pump current and feedback strength. The 2τ peak is chosen because, as mentioned in the previous section, it is the largest, which is typical of PROF systems. Nevertheless, we have verified that the first peak at τ delay shows the same features. The results are shown in Fig. 3.9. Pump current is on the horizontal axis, feedback strength is along the vertical, and

the 2τ AC peak height is indicated by the color legend on the right hand side.

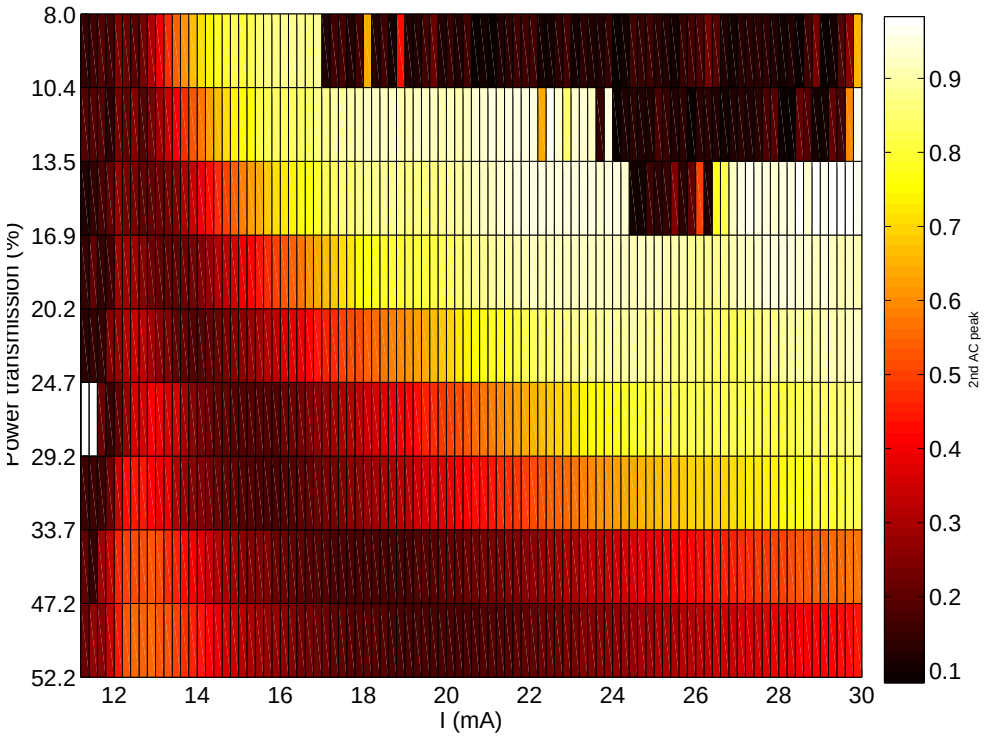

Figure 3.9: Map of AC peak height for varying feedback and current conditions.

A region of low AC appears abruptly for low coupling (power transmission of around 16.9%)and high current (24 mA), but this is a region of steady-state operation. The low AC in this case arises from noise, and so is rejected for a dynamics-based random bit generator. Similarly, a thin ribbon of low AC appears at the lowest currents (under 12 mA), but here the laser operates below threshold so the conditions are similarly unsuitable. However, a wedge of low AC begins at low current (13 mA) and low coupling (10.4% of power transmission), but smoothly grows and expands into a larger region of high feedback strength (power transmission of around 52.2%) and moderate currents (between 16-23 mA). This region also displays a broad RF spectrum, and so is identified as the most promising region for random bit sequences generation purposes. We emphasize that it is not obvious a priori that the AC properties would change with current, showing a local minimum that depends on the feedback strength.

Based on the dynamical guidance provided by the combination of a broad RF spectra (as presented in Figures 3.4 (b) or (d)) and AC characteristics with short delay peaks (feedback strength and pumping current conditions inside the wedge), we select a pump current I = 19.00 mA and feedback T = 52.2 % as our operating point for a random number generator based on chaotic laser dynamics (see Chapter 4).

4

Application to random bit generation

Random bit generators (RBGs) are key components of several digital technologies, including encryption and authentication protocols, stochastic modeling, and online gaming and lotteries [36]. Quantum RBGs promise to generate truly sequences based on truly random processes [37], but typically produce them too slowly to keep pace with modern data rates. In contrast, pseudorandom bit generators based on a random seed and a deterministic algorithm are well known, but are vulnerable if the seed can be guessed. A new approach that has attracted attention is to digitize an analog noise [38] or chaotic signal [20], taking advantage of the inherent noise in combination with chaos-induced decorrelation of the trajectory as the basis for the generation of independent bits. Semiconductor lasers are an excellent source for this technique. Their short internal timescales allow for large bandwidth dynamics when subjected to external perturbations. Delayed optical feedback as an external perturbation can induce strongly diverging chaotic trajectories, thus making rapid bit rates possible [39] [40].

In this chapter we consider a laser system with polarization-rotated optical feedback and the digitization procedures and randomness properties of the acquired data from this system. Standard test batteries [41] provide statistical evidence of the randomness of a candidate bitstream. They represent the reference for randomness and can be computationally intensive and time consuming. In order to construct or identify suitable systems for RBG, it is mandatory to understand the conditions under which a dynamical system and digitization process are likely to succeed or fail, without having to test all possible conditions in advance. In chapter 3, we examined the dynamics of a chaotic semiconductor laser to determine an optimum regime for producing random bit streams. The subject of this chapter is to consider the interplay between the dynamics and the digitization process, and show that competitive bit rates can be achieved using an 8-bit analog-to-digital converter (ADC) and minimum postprocessing. The content of this chapter is an extension of the work we presented in [42].

4.1 Digitization procedures

Digitization procedures are necessary to achieve a sequence of random bits from an analog dynamic system. These procedures include a variety of postprocessing methods, which are always desirable to be minimized, not only to keep most of the original information, but also to not slow down the process when implemented in real time. In our case, two main operations are carried out to the detected laser output: acquisition of points, which includes analog to digital conversion, and truncation of bits.

4.1.1 Criteria for sampling rate and data acquisition

The sampling rate is a crucial parameter for random bit generation, since the final bit rate depends strongly on the time scales of the dynamical system and the initial sampling rate of the oscilloscope. The larger the sampling rate is, the more it becomes possible to generate bits at higher speed.

The first step we carry out is to capture time series at a 40 GS/s sampling rate with the oscilloscope (LeCroy 816Zi, 16 GHz analog bandwidth, 8-bit ADC) under the operating conditions we selected in the previous chapter, pump current I = 19.00 mA and feedback T = 52.2 % (see Section 3.4). The full sampling rate is used to avoid undesired frequency filtering which is enforced by the Digital Signal Processing (DSP) when lower rates are used. The oscilloscope saves data initially in 16-bit binary word format, which we truncate to the 8 most significant bits (MSBs) to equal the raw ADC resolution.

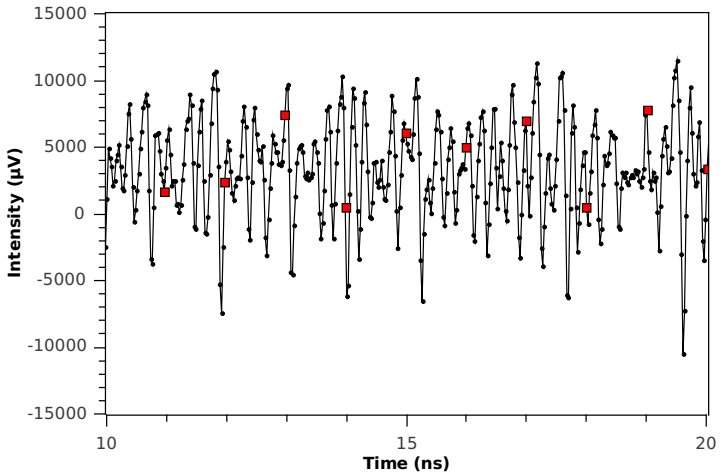

Figure 4.1. Chaotic oscillations in the output intensity of a SL pumped at $1.52I_{th}$ with PROF. Red squares indicate the points used for random bit generation.

The procedure we perform to the 8-bit raw data is the extraction of points

separated by a 1 ns interval. In this manner, the chosen set of points exceed the decay time of the zeroth AC peak, which is around 0.7 ns (see Fig. 3.8 (a)), and therefore we ensure that points forming the new signal are not correlated. This new set of points does not depend on past inputs and it is said to have no memory, which makes it more suitable for random bit generation. In Figure 4.1 the red colored squares indicate data separated 1 ns in time, which written in 8-bit format as presented in Table 4.1 will be used to generate random bits. Note that the first three bit positions in the ten binary numbers present almost no variation. Avoiding this fact is crucial for RBG, as explained in the next subsection.

Binary number								
1	0	0	0	0	0	1	1	0
2	0	0	0	0	1	0	0	1
3	0	0	0	1	1	1	0	0
4	0	0	0	0	0	0	0	1
5	0	0	0	1	0	1	1	1
6	0	0	0	1	0	0	1	1
7	0	0	0	1	1	0	1	1
8	0	0	0	0	0	0	0	1
9	0	0	0	1	1	1	1	0
10	0	0	0	0	1	1	0	1

Table 4.1: Table containing binary numbers from Figure 4.1 spaced 1 ns in time used for RBG.

4.1.2 Truncation of bits

A point of emphasis in our study is to minimize postprocessing requirements as much as possible, to demonstrate the efficacy of methods based on the dynamics to generate randomness. This is in contrast to protocols which start with a chaotic signal, but significant manipulation of the data is also employed, such as additional logical or software processing which combines outputs through logic gates or computing high-order derivatives [43]. Our approach is to simply omit some of the Most Significant Bits (MSBs) from each acquired data point (sample). The most significant bits are the bit positions in a binary number representing the higher exponents of 2. Fig. 4.2 shows decimal 75 in its binary representation with the 2 MSBs highlighted.

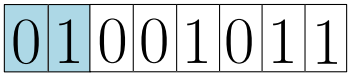

Figure 4.2: Binary representation of number 75 with the 2 MSBs colored in blue.

The original chaotic laser intensity does not cover all values with equal probability. This can be observed from Fig. 4.3 which shows a histogram for the laser

signal, without the omission of any MSB. The horizontal axis, named index, indicates the 2^8 different values one can create with 8 bits. The distribution resembles a Gaussian, in which certain values are clearly more likely to occur than others.

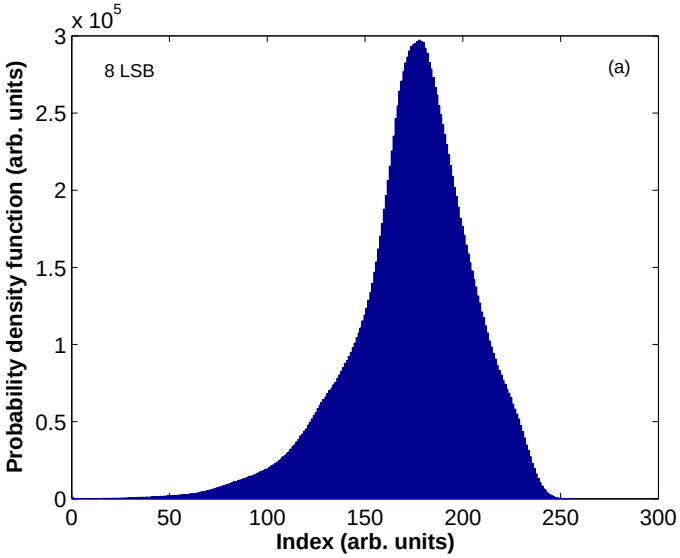

Figure 4.3. Probability density function for 8 bits, obtained at pump current I=19.00 mA and feedback T=52.20 %.

To compensate for this unequal distribution in the parent distribution of points we exclude the MSBs. This truncation of bits can also remove the residual correlations present in the original dynamics. The number of bits necessary to remove can be estimated by plotting histograms of the truncated values until a flat histogram within allowed statistical variation is obtained. Fig 4.4 shows the distribution for 7- to 4- bit samples from one chaotic waveform acquired under the selected optimum conditions (pump current I=19.00 mA and feedback T=52.2%) Again, the x axis represents the 2^{LSB} possible values. The largest MSB is omitted in Fig. 4.4 (b), showing the seven least significant bits. Still. there is a clear peak in the histogram. In Figure 4.4 (c) two of the most significant bits are excluded. The probability distribution becomes more uniform while its maximum starts to vanish. When only the five least significant bits are selected the histogram becomes flatter, as figure 4.4 (d) indicates. Keeping the 4 LSB of the 8-bit data, the distribution looks uniform (Figure 4.4 (e)).

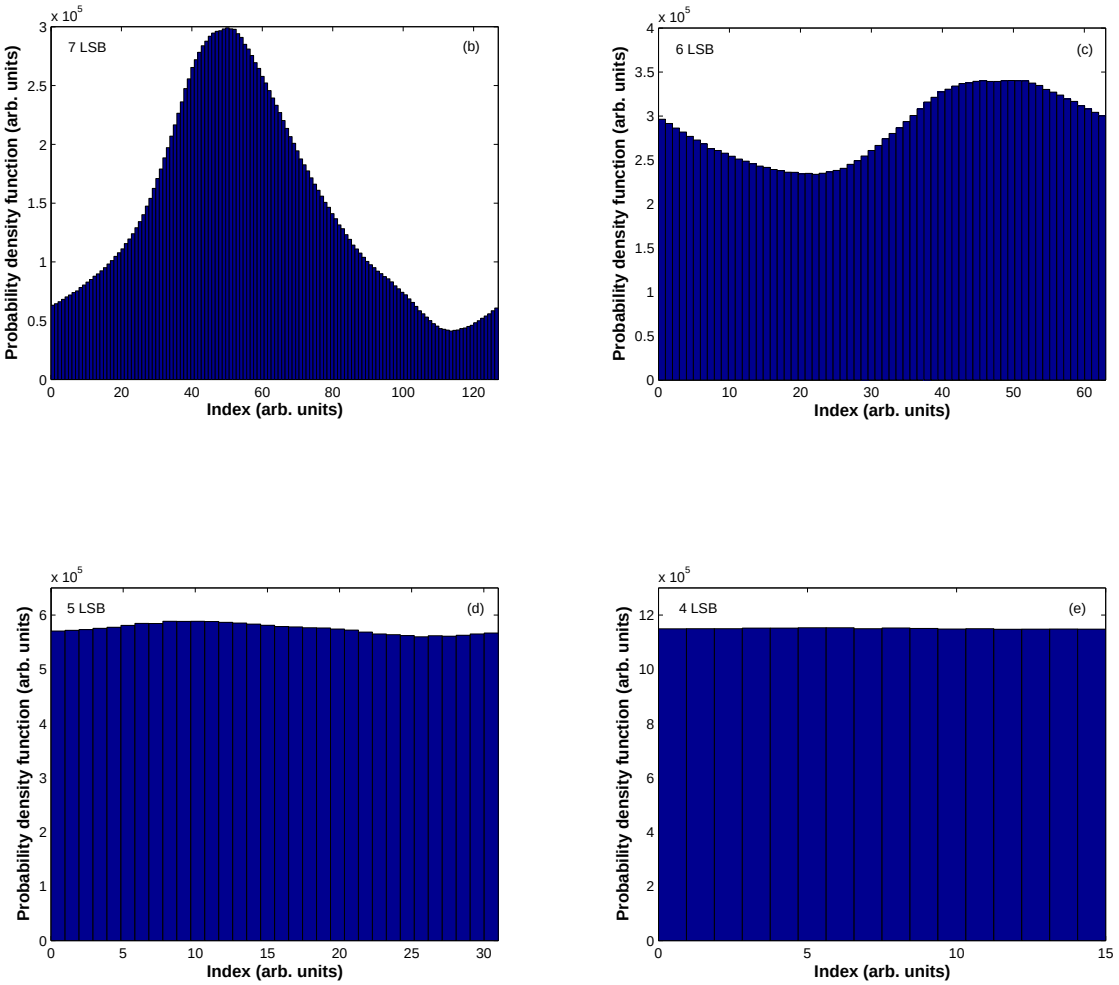

Figure 4.4. Probability density functions for (b) 7 LSBs, (c) 6 LSBs, (d) 5 LSBs and (e) 4 LSBs.

4.1.3 Study of the bias

To complete the study, we can examine the bias from the equiprobable distribution of each significant bit. The bias can be defined as the deviation of the probability of obtaining a bit 1 with respect to the expected probability (0.5) for each bit position of the binary number. To do this, we calculate the bias B_i for significant bit i (i = 1 indicates the LSB while i = 8 the MSB) as:

$$B_i = P_i - 0.5 \tag{4.1}$$

where P_i is the probability of obtaining a bit 1 for a given significant bit. Smaller values of B_i imply more randomness, so large bias of a bit indicates it might be unsuitable for random bit generation.

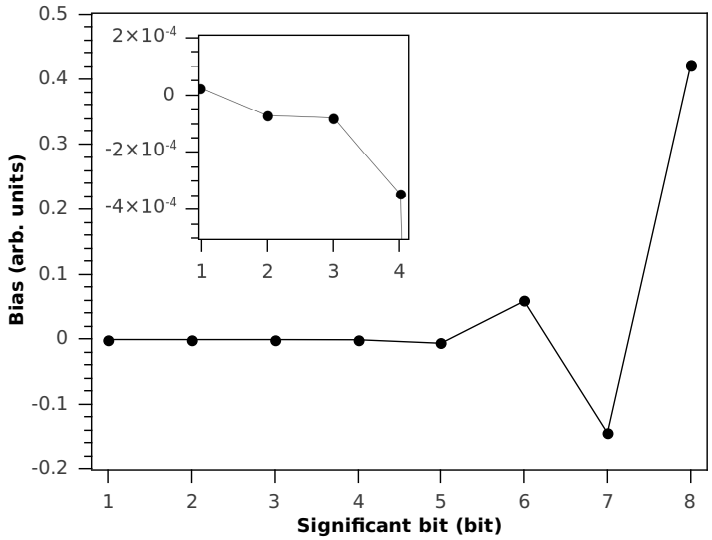

Figure 4.5: Bias of each significant bit.

Figure 4.5 shows the calculated bias of each significant bit for 20 million binary numbers. The binary numbers are samples spaced 1 ns in time from time traces obtained under the same conditions (pump current I = 19.00 mA and feedback T = 52.2%). The bias increases with i, having the MSB (i=8) the largest bias value. It is worth mentioning that the cases with i=2, i=3, i=4, i=5, i=7 significant bits have a defect of bits 1, while i=1, i=6 and i=8 have an excess of 1s. The inset of Fig. 4.5 depicts a magnification of the bias for the four LSBs.

The guiding bias is $1/\sqrt{N}$, where N represents the length of the binary numbers. In this particular case, the bias should be $\leq 2.3 \cdot 10^{-4}$, meaning that larger bias might not be appropiate to generate good-quality random bits. After perfoming this analysis, the four MSBs are discarded from each 8-bit sample, and the four least significant bits (LSBs) are retained, as illustrated in Figure 4.6. The bits obtained in this manner from points originally separated 1 ns in time, form the bitstream that we evaluate for randomness using the NIST battery of statistical tests, explained in the next section.

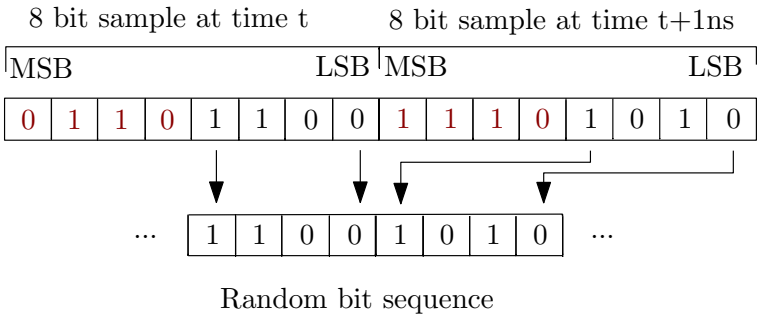

Figure 4.6: Illustration of the method used to generate the random bitstream.

Moreover, other aspects of the digitization conditions are also important. In addition to sampling rate considerations and bit truncation, the vertical digitization conditions, intrinsic to the acquisition hardware, are also critical to successful random bit generation. Specifically, it is necessary to use the full 8-bit range as much as possible, while avoiding conditions where the acquired signal exceeds the specified vertical scale. If there are too many points that go off-scale, the oscilloscope simply records them as the extrema values, thus producing certain strings of consecutive ones or zeros too frequently; these flawed bitstrings typically fail some randomness tests as discussed below. A signal too small will only span a small subset of the possible 8-bit range and become more likely to fail as well. These competing demands must be balanced as much as possible. This can be done by scaling the input analog amplitude to match the vertical range, and compensating for vertical asymmetry. We avoided the variable gain feature of the scope which can lead to a skewed distribution of values due to the software processing.

4.2 NIST battery of statistical tests

The National Institute of Standards and Technologies (NIST) provides a Statistical Test Suite for Random and Pseudorandom Number Generators for Cryptographic Applications [41]. This Test Suite consists of 15 tests that were developed to verify the randomness of a bit sequence generated by random or pseudorandom number generator. In Table 4.2, the 15 NIST tests and a short description of their main purpose of each test is provided. For an in-depth description, please see [41].

Each test is based on a calculated statistical value known as the p-value. The p-value is the probability that a perfect random bit generator would have produced a sequence less random than the sequence being tested, given the kind of nonrandomness assessed by the test. Consequently, a p-value equal to 1 implies that the sequence appears to be totally random, while a p-value equal to 0 indicates that the sequence is completely non-random. A significant level (α), typically chosen in the range [0.001,0.01], can be defined for the tests. In our case we choose α=0.01, indicating that one would expect 1 sequence in a hundred to be rejected. In our case, the p-value of the uniformity of p-values should be larger than 0.0001 to pass all the tests.

4.3 Results

A bitstream formed from points acquired at a pump current of 19.00 mA and feedback strength of T = 52.2 % is tested using the NIST tests. As explained in previous sections, points are separated by 1 ns and truncated to the 4 LSB to ensure the absence of correlations and a uniform probability density function.

Statistical Test	**Test Purpose**
The Frequency (Monobit) Test	Determine whether the number of zeros and ones are approximately the same as would be expected for a truly random sequence.
Frequency Test within a Block	Determine whether the frequency of ones in an M-bit block is approximately M/2.
The Runs Test	Determine whether the number of runs (k identical bits bounded by opposite bits) of ones and zeros of different k is as expected for a random sequence.
Test for the Longest-Run-of-Ones in a Block	Determine whether the length of the longest run of ones within the tested sequence is consistent with the expected length in a random sequence.
The Binary Matrix Rank Test	Check for linear dependence among fixed length substrings of the original sequence.
The Discrete Fourier Transform (Spectral) Test	Detect periodic features in the tested sequence.
The Non-overlapping Template Matching Test	Detect generators that produce too many occurrences of a given aperiodic pattern.
The Overlapping Template Matching Test	Detect generators that produce too many occurrences of a given aperiodic pattern.
Maurer's "Universal Statistical" Test	Detect whether the sequence can be significantly compressed without loss of information.
The Linear Complexity Test	Determine whether the sequence is complex enough to be considered random.
The Serial Test	Determine whether the number of occurrences of the 2^m m-bit overlapping patterns is approximately the same as expected for a random sequence.
The Approximate Entropy Test	Compare the frequency of overlapping blocks of 2 consecutive lengths (m and m+1) with the expected result for a random sequence.
The Cumulative Sums Test	Test whether the cumulative sum of partial sequences occurring in the tested sequence is too large or too small relative to the expected for random sequences.
The Random Excursions Test	Determine if the number of visits to a particular state within a cycle deviates from what expected for a random sequence.
The Random Excursions Variant Test	Detect deviations from the expected number of visits to various states in a random walk.

Table 4.2: Description of the purposes for each NIST test. Extracted and adapted from [41].

The results of the NIST battery are shown in Table 4.3. for 1000 samples of 1 million bits each. For tests which produce multiple p-values, the worst case is shown. All tests pass, verifying that under these conditions our system and procedure produce a statistically random bitstream. The bit rate is 4 Gbit/s, based on four bits per data point and a 1 ns interval between points. This speed is competitive with recent work in other systems. It is not a full real-time implementation, but a demonstration of this system/s capability.

Statistical Test	**P-value (min)**	**Result**
Frequency	0.033584	Success
Block Frequency	0.851383	Success
Runs	0.090388	Success
Longest-Run-of-Ones	0.227180	Success
Rank	0.371941	Success
Discrete Fourier Transform	0.699313	Success
Non-overlapping Template	0.013102	Success
Overlapping Template	0.044797	Success
Maurer's Universal	0.419021	Success
Linear Complexity	0.701366	Success
Serial	0.180568	Success
Approximate Entropy	0.394195	Success
Cumulative Sums	0.179584	Success
Random Excursions	0.126609	Success
Random Excursions Variant	0.066528	Success.

Table 4.3. Results of Statistical Test Suite NIST SP800-22 for a set of 1000 Sequences of 1Mbit each

4.4 Role of postprocessing

So far we have relied on dynamical properties to generate random numbers. The result has been satisfactory, generating bitstreams capable to pass the NIST battery of tests at a rate of 4 Gbit/s. In this section we try to understand in more detail the role played by postprocessing methods, in order to increase the generation bit rate.

4.4.1 Dependence on the number of LSB used

We first investigated the dependence of failed NIST tests on the number of LSBs used as random for 1Gbit data. The data used correspond again to samples separated 1 ns and acquired under conditions selected as optimum (pump current of 19.00 mA and feedback strength of T = 52.2 %). Figure 4.7 shows the number of failed NIST

tests as a function of the number of LSBs, ranging from 4 to 8 which correspond to all bits including the MSB. For 5 LSBs, five are the tests that don't succeed (Frequency, Cumulative Sums, Runs, Non Overlapping Template and Approximate Entropy) and the number of failed tests increases with the number of bits used. This result is consistent with the analysis presented in section 4.1.2. and confirms that the maximum number of LSBs we can utilize as random without any extra postprocessing method is 4 LSBs, resulting in a generation rate of 4Gbit/s.

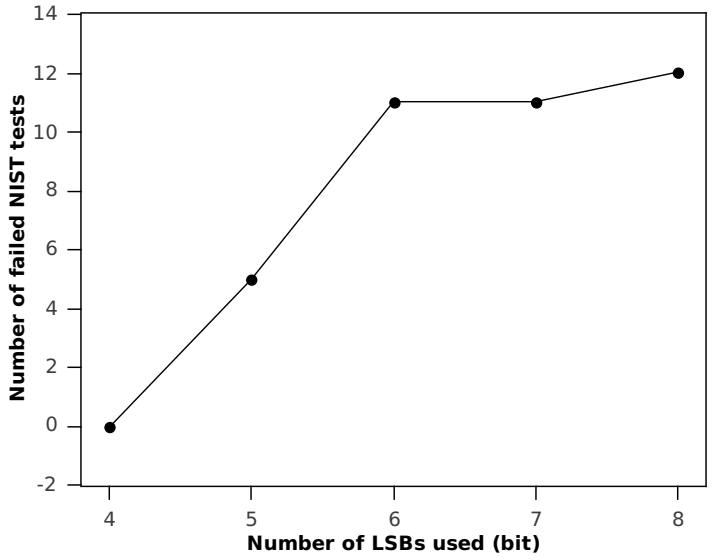

Figure 4.7: Dependence of the randomness on the number of LSBs used.

4.4.2 Dependence on the dynamical conditions

To gain more insight, we performed the same procedure for operating conditions other than the optimal case in the wedge of low AC region (marked in light yellow in Fig.3.9.) and near its periphery. For a 1Gbit sequence, we find that some conditions in this wedge other than the optimal case (such as I = 17 mA and T = 52.2% or = 16 mA and T = 33.7%) fail a few NIST tests, typically the Frequency or Runs tests. These failures might be avoided, as explained in section 4.1, adjusting properly the amplitude of the analog signal to the vertical scale of the oscilloscope. This means filling the 8-bit range as much as possible but without recording points in saturation.

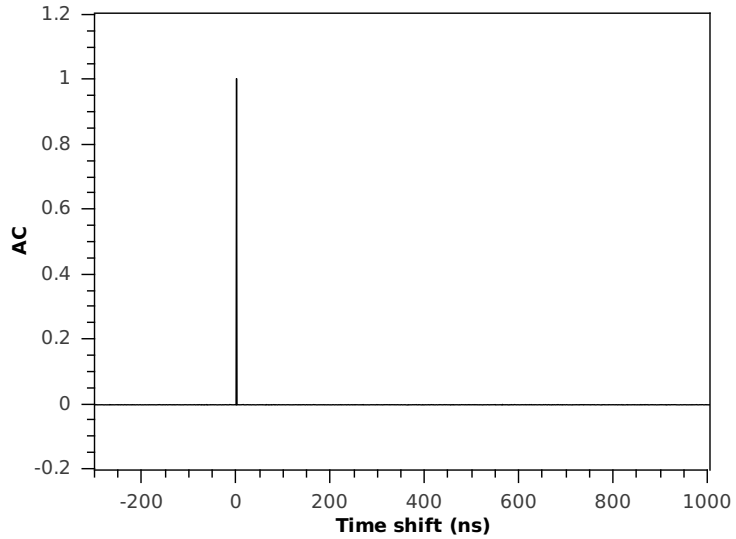

Figure 4.8: AC of a signal with 4 LSB obtained at I=19.00mA and T=16.9%

We also analyzed conditions outside the main region of low AC (I = 22.00 mA and T = 20.2% and I=19.00 mA and T=16.9%). Surprinsingly, for the latter case, we passed all randomness tests despite the clearly existing long-range correlations. Figure 4.8. shows the AC function of a signal obtained under conditions similar to the case presented in Figure 3.7 (f), I = 19 mA and T = 16.9%, but only with its 4 LSBs. The truncation of 4 bits causes the total extinction of the AC peaks at integer multiples of τ, showing a AC function equal to zero except for t=0. This example indicates that the omission of the 4 MSBs represents a postprocessing procedure that can compensate for some residual correlations.

4.4.3 Dependence on the acquisition conditions

In an attempt to study the full potential of the system and based on the total extinction of the AC peaks shown in Fig. 4.8, we have followed a new approach. We wanted to explore the capabilities of our experimental setup, finding out which is the maximum bit generation rate obtainable with this system, taking into account that the omission of the 4 MSB seems enough postprocessing to reduce correlations. Therefore, our proposal was to use all samples from the original signal separated 25 ps in time and obtained at the optimum condition (I = 19.00 mA and T = 52.20 %) for RBG and repeat the same procedure explained in the preceding sections. We first truncated the bits from the initial signal to its 4 LSBs. The histogram for the 4 LSBs is shown in Figure 4.9. Again, the probability distribution seems flat and uniform.

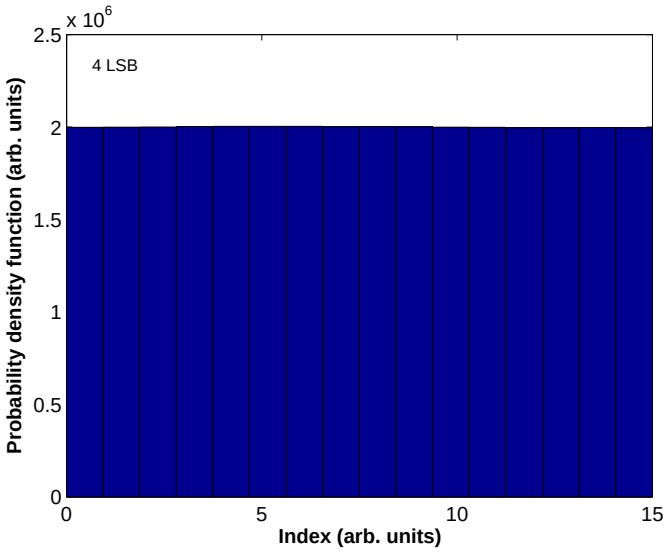

Figure 4.9: Probability density function for 4 LSBs from the original signal.

We then confirmed that there are no correlations in the signal regardless of the short time between samples (25 ps). Figure 4.10 shows the AC function of the original signal without the 4 MSBs. Again, the peaks at integer multiples of τ disappear, showing that in this case, it is not necessary to create a new set of points separated by a time larger than the decay time of the zeroth AC peak.

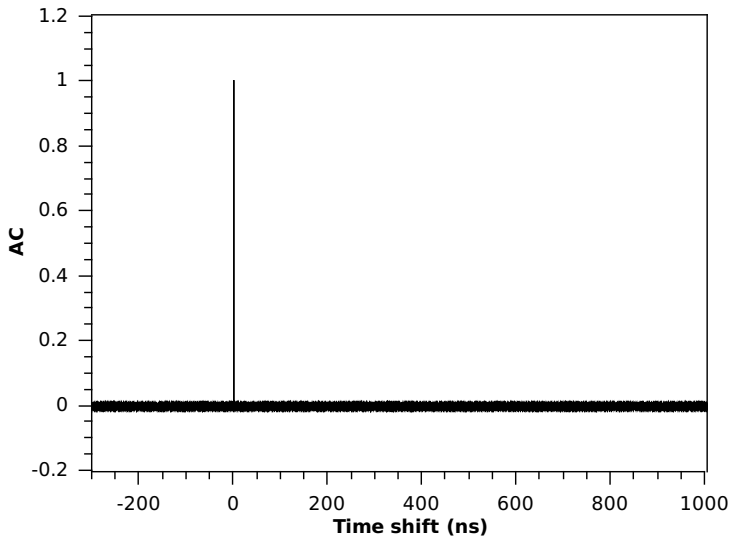

Figure 4.10: AC of the original signal with 4 LSB obtained at I=19.00mA and T=16.9%

A bitstream of 1Gbit, acquired at the optimum condition I = 19.00 mA and T = 52.20 %, underwent the NIST tests. The results, shown in Table 4.4, prove that we suceeded in passing all the 15 NIST tests. The obtained bit rate is in this

case 160 Gbit/s, based on four bits per data point and a 25 ps interval between points. This example shows that the exclusion of the 4 most significant bits might be a sufficient postprocessing method for RBG and we might not need to perform other procedures that could slow down the system when implemented in real-time. Such a high bit rate is (160 Gbit/s), achieved from a compact system and with bit truncation as the only postprocessing method, has not been previously reported in the literature.

Statistical Test	**P-value (min)**	**Result**
Frequency	0.102526	Success
Block Frequency	0.005017	Success
Runs	0.975644	Success
Longest-Run-of-Ones	0.010911	Success
Rank	0.842937	Success
Discrete Fourier Transform	0.792508	Success
Non-overlapping Template	0.000775	Success
Overlapping Template	0.439122	Success
Maurer's Universal	0.968863	Success
Linear Complexity	0.390721	Success
Serial	0.461612	Success
Approximate Entropy	0.500279	Success
Cumulative Sums	0.162606	Success
Random Excursions	0.155328	Success
Random Excursions Variant	0.130111	Success.

Table 4.4. Results of Statistical Test Suite NIST SP800-22 for a Set of 1000 Sequences of 1Mbit each

We can conclude that, to generate random bits, dynamical properties, acquisition conditions and postprocessing all play important roles and a delicate balance between them is crucial for the success. We have presented a simple, robust, and versatile semiconductor laser system and proved that its chaotic dynamics can be used for random bit generation. We have also shown how to use its dynamics for guidance to identify optimal operating regimes and digitization conditions for random bit generation. Using these methods and minimal postprocessing, we extract a statistically random bitstream at a rate of 4 Gbit/s and up to 160 Gbit/s.

5

Summary and Outlook

In this MS Thesis we have conducted an experimental study of the dynamical properties of a semiconductor laser subjected to delayed optical feedback, specifically polarization rotated optical feedback (PROF). Tailoring such dynamical properties has been fundamental to use our experiment for a current application of growing interest: the generation of random bits.

Our experiment, carried out in the Nonlinear Photonics Laboratory of IFISC, began with a thorough characterization of the solitary edge-emiting laser. The said semiconductor laser was used in a delayed optical feedback setup, where a Faraday Mirror rotated the polarization state of the light by 90° originating PROF. We discussed the main properties of the dynamical characteristics of a semiconductor laser subjected to PROF, presenting a new systematic study that allowed us to identify the optimum operating conditions for the generation of random bits. We also observed that successful random bit generation is very sensitive to digitization and postprocessing procedures. Applying the identified criteria, we achieved high random bit generation rates. Futhermore, we demonstrated that with proper balance between the dynamics, acquisition conditions and postprocessing methods, the generation bit rate can be improved from 4 Gbit/s to 160 Gbit/s. However, we would like to stress, that this work goes beyond the mere reporting of a certain high bit rate and aims for three major advances:

1. Implementing a simple, robust and low-cost system, completely made of standard telecom components.

2. Making steps towards an understanding of the existing requirements for the underlying dynamics, and therefore which dynamical properties are more favorable for random bit sequence generation.

3. How the detection and digitization procedures interfere and limit the obtainable bit rates, even when using only the most basic postprocessing.

We think that after the first successful reports, underlining the potential of

chaotic optical systems for high bit rate random number generators, it is essential to gain a deeper understanding of the involved processes. This is where this work contributes significantly and the aim is to use the capability of these systems optimally.

Future work will concentrate, on the one hand, on the optimization of the number of bits used without increasing the postprocessing steps. For this aim, new postprocessing techniques, like bit order reversion of the signal, might be a good strategy. Reducing the time step between samples can also improve the final bit rate. But in this regard, the technological evolution plays a role, since the generation bit rates depend directly on the sampling capability of the future oscilloscopes.

On the other hand, a rate equations model able to reproduce the different dynamical ranges present in a laser system subjected to PROF is still missing. The derivation of a new model, which considers not only the TE to TM mode injection but also the case where TM is injected to TE mode, could lead through numerical simulations to a better understanding of PROF systems. The influence of delay on PROF systems is still poorly understood. Issues such as the interaction of the fed back light with the optical field or the polarization modes involved in the emission, are under active investigation. Therefore, PROF dynamics has turned into an interesting example of intriguing delay dynamics.

Moreover, there are still some open questions related to laser-based random bit generators. Although a first approach has been reported recently [44], it is still unclear how the entropy of bits depends on the inherent noise and the dynamical properties of the laser. Furthermore, and for secure communication purposes, a theoretical method, where two RBGs based on mutually coupled chaotic lasers are synchronized, was proposed in 2010 [45]. A first experimental implementation was reported recently by Yoshimura et. al [46] with generation rates of 2Mbit/s. Whether secure synchronization of two RBGs at faster synchronization times is experimentally possible remains an exciting challenge for the future.

Bibliography

[1] C. R. Mirasso, P. Colet, and P. Garcia-Fernandez, *Synchronization of Chaotic Semiconductor Lasers: Application to Encoded Communications*, IEEE Photonics Technology Letters, Vol. **8**, 299 (1996).

[2] J. Mork, P. Christiansen, and B. Tromberg *Bistability and low-frequency fluctuations in semiconductor lasers with optical feedback: A theoretical analysis*, IEEE Journal of Quantum Electronics, Vol. **24**, 123-133 (1988).

[3] D. Lenstra, B.Verbeek, and A. Den Boef *Coherence collapse in single-mode semiconductor lasers due to optical feedback*, IEEE Journal of Quantum Electronics, Vol. **21**, 674-679 (1985).

[4] T. Heil, I. Fischer,W. Elsäßer, and A. Gavrielides *Dynamics of Semiconductor Lasers Subject to Delayed Optical Feedback: The Short Cavity Regime*, Physical Review Letters, Vol. **87**, 24, 243901 (2001).

[5] W. H. Loh, Y. Ozeki, and C. L. Tang *Highâfrequency polarization selfâmodulation and chaotic phenomena in external cavity semiconductor lasers*, Applied Physics Letters, Vol. **56**, 26, 2613 (1990).

[6] J. F. Dynes, Z. L. Yuan, A. W. Sharpe, A. J. Shields *A high speed, postprocessing free, quantum random number generator*, Applied Physics Letters, Vol. **93**, 031109 (2008).

[7] A. R. Dixon, Z. L. Yuan, J. F. Dynes, A. W. Sharpe, A. J. Shields *Gigahertz decoy quantum key distribution with 1Mbit/s secure key rate*, Optics Express, Vol. **16**, 23, 18790-19797 (2008).

[8] A. Argyris, S. Deligiannidis, E. Pikasis, A. Bogris, and D. Syvridis *Implementation of 140 Gb/s true random bit generator based on a chaotic photonic integrated circuit*, Optics Express, Vol. **18**, 18, 18763-18768 (2010).

[9] H. Guo, W. Tang, Y. Liu and W. Wei, *Truly random number generation based on measurement of phase noise of a laser*, Physical Review E, Vol. **81**, 051137 (2010).

[10] K. Hirano, T. Yamazaki, S. Morikatsu, H. Okumura, H. Aida, A. Uchida, S. Yoshimori, K. Yoshimura, T. Harayama and P. Davis *Fast random bit generation with bandwidth-enhanced chaos in semiconductor lasers*, Optics Express, Vol. **18**, 6, 5512-5524 (2010).

[11] R. N. Hall, G. E. Fenner, J. D. Kingsley, T. J. Soltys, R. O. Carlson, *Coherent light emission from GaAs junctions*, Physical Review Letters, Vol. **9**, 366-369 (1962).

[12] J. Hecht, *Understanding Lasers: An Entry-Level Guide*, 3rd Ed. John Wiley] & Sons, (2008).

[13] H. Soda, K. Iga, C. Kitahara, and Y. Suematsu, *GaInAsP/InP surface emitting injection lasers*, Jpn. J. Appl. Phys., Vol. **18**, 12, 2329-2330 (1979).

[14] A. K. Jansen van Doorn, M. P. van Exter, A. M. van der Lee, and J. P. Woerdman, *Coupled-mode description for the polarization state of a vertical cavity semiconductor laser*, Phys. Rev. A, Vol. **55**, 1473â1484 (1997).

[15] A. Jansen van Doorn, M. van Exter, and J. Woerdman, *Elasto-optic anisotropy and polarization orientation of vertical-cavity surface-emitting semiconductor lasers*, Applied Physics Letters, Vol. **69**, 8, 1041â1043, (2006).

[16] R. Lang, K. Kobayashi, *External optical feedback effects on semiconductor injection laser properties*, IEEE Journal of Quantum Electronics, Vol. **16**, 3, 347-355 (1980).

[17] R. Tkach, A. Chraplyvy, *Regimes of feedback effects in 1.5-μm distributed feedback lasers*, J. Lightwave Technol., Vol. **4**, 11. 1655-1661 (1986).

[18] A. Argyris, D. Syvridis, L. Larger, V. Annovazzi-Lodi, P. Colet, I. Fischer, J. García-Ojalvo, C. R. Mirasso, L. Pesquera, K. A. Shore, *Chaos-based communications at high bit rates using commercial fiber-optic links*, Nature, Vol. **348**, 343-346 (2005).

[19] F. Y. Lin, J. M. Liu, *Chaotic lidar*, IEEE J. Sel. Top. Quantum Electron., Vol. **10**, 991-997 (2004).

[20] A. Uchida, K. Amano, M. Inoue, K. Hirano, S. Naito, H. Someya, I. Oowada, T. Kurashige, M. Shiki, S. Yoshimori, K. Yoshimura, P. Davis, *Fast physical random bit generation with chaotic semiconductor lasers*, Nature Photonics, Vol. **2**, 728-732 (2008).

[21] T. Heil, A. Uchida, P. Davis, T. Aida, *TE-TM dynamics in a semiconductor laser subject to polarization-rotated optical feedback*, Phys. Rev. A, Vol. **68**, 033811 (2003).

[22] J. Ohtsubo, *Semiconductor lasers: stability, instability and chaos*, 2nd Ed. Springer, Berlin (2007).

[23] H. Li, A. Hohl, A. Gavrielides, H. Hou, K. D. Choquette, *Stable polarization self-modulation in vertical-cavity surface emitting lasers*, Applied Physics Letters, **72**, 19, 2355-2357 (1998).

[24] D. W. Sukow, A. Gavrielides, T. Erneux, B. Mooneyham, K. Lee, J. McKay, J. Davis, *Asymmetric square-waves in mutually-coupled semiconductor lasers with orthogonal optical injection*, Physical Review E, Vol. **81**, 025206R (2010).

[25] K. Otsuka, J-L Chern, *High-speed picosecond pulse generation in semiconductor lasers with incoherent optical feedback*, Opt. Lett. **16**, 1759-1761 (1991).

[26] W. L. Zhang, W. Pan, B. Luo, X. F. Li, X. H. Zuo, M. Y. Wang, *Theoretical study on polarization dynamics of VCSELs with negative optoelectronic feedback*, Applied Optics, Vol. **46**, 29, 7262-7266 (2007).

[27] J. Houlihan, G. Huyet, J.G. McInerney, *Dynamics of a semiconductor laser with incoherent optical feedback*, Opt. Commun. 199, 175-179 (2001).

[28] R. Ju, P.S. Spencer, *Dynamic regimes in semiconductor lasers subject to incoherent optical feedback*, Journal of Lightwave Technology, vol.**23**, 8, 2513- 2523, (2005).

[29] R. Ju, Y. Hong, P.S. Spencer, *Semiconductor lasers subject to polarisation-rotated*

optical feedback, IEE Proc. Optoelectron. **153**, 3, 131-137 (2006).

[30] D. Cheng, T. Yen, J. Chang, J. Tsai, *Generation of high-speed single-wavelength optical pulses in semiconductor lasers with orthogonal- polarization optical feedback*, Optics Communications **222**, 363-369 (2003).

[31] I. Fischer, T. Heil, W. Elsäßer, *Fundamental Issues of Nonlinear Laser Dynamics*, AIP Conf. Proc. No. 548, p.218 (AIP, Melville, NY, 2000).

[32] M. Peil, I. Fischer, W. Elsäßer, *A short external cavity semiconductor laser cryptosystem*, C. R. Physique, vol. **5** No. 6, 633-642 (2004).

[33] I. Fischer, Y. Liu, P. Davis *Synchronization of chaotic semiconductor laser dynamics on subnanosecond time scales and its potential for chaos communications*, Phys. Rev. A, vol. **62** 011801 (2000).

[34] L. Larger, J.-P. Goedgebuer, *Encryption using chaotic dynamics for optical telecommunications*, C. R. Physique, vol. **5** (2004).

[35] M. Peil, I. Fischer, W. Elsäßer, S. Bakic, N. Damaschke, C. Tropea, S. Stry, J. Sacher, *Rainbow refractometry with a tailored incoherent semiconductor laser source*, Appl. Phys. Lett., vol. **89** 091106 (2006).

[36] N. Ferguson, B. Schneier, T. Kohno, *Cryptography Engineering: Design Principles and Practical Applications*, Wiley (20010).

[37] C. Gabriel, C. Wittman, D. Sych, R. Dong, W. Mauerer, U. L. Anderson, C. Marquardt, G. Leuchs, *A generator for unique quantum random numbers based on vacuum states*, Nature Photonics., vol. **4** 711-715 (2010).

[38] X. Li, B. Cohen, T. E. Murphy, R. Roy, *Scalable parallel physical random number generator based on a superluminescent LED*, Opt. Lett., vol. **36** 1020-1022 (2011).

[39] I. Reidler, Y. Aviad, M. Rosenbluh, I. Kanter, *Ultrahigh-speed random number generation based on a chaotic semiconductor laser*, Physical Review Letters, vol. **103** 024102 (2009).

[40] A. Argyris, S. Deligiannidis, E. Pikasis, A. Bogris, D. Syvridis, *Implementation of 140Gb/s true random bit generator based on a photonic integrated circuit*, Optics Express, vol. **18** 18768 (2010).

[41] A. Rukhin, J. Soto, J. Nechvatal, M. Smid, E. Barker, S. Leigh, M. Levenson, M. Vangel, D. Banks, A. Heckert, J. Dray, S. Vo, *A Statistical Test Suite for Random and Pseudorandom Number Generators for Cryptographic Applications*, NIST Special Publication 800-22, Revision 1a (2010).

[42] N. Oliver, M. C. Soriano, D. W. Sukow, I. Fischer, *Dynamics of a semiconductor laser with polarization-rotated feedback and its utilization for random bit generation*, Optics Letters, vol. **36** No. 23, 4632-4634 (2011).

[43] I. Kanter, Y. Aviad, I. Reidler, E. Cohen, M. Rosenbluh, *An optical ultrafast random bit generator*, Nature Photonics, vol. **4** 58-61 (2010).

[44] T. Mikami, K. Kanno, K. Aoyama, A. Uchida, T. Ikeguchi, T. Harayama, S. Sunada, K. Arai, K. Yoshimura, P. Davis *Estimation of entropy rate in a fast physical random-bit generator using a chaotic semiconductor laser with intrinsic noise*, Physical Review E, vol. **85**, 016211 (2012).

[45] I. Kanter, M. Butkovski, Y. Peleg, M. Zigzag, Y. Aviad, I. Reidler, M. Rosenbluh, W. Kinzel *Synchronization of random bit generators based on coupled chaotic lasers and*

application to cryptography, Optics Express, vol. **18**, No. 17, 18292-18302 (2010).

[46] K. Yoshimura, J. Muramatsu, P. Davis, T. Harayama, H. Okumura, S. Morikatsu, H. Aida, A. Uchida, *Secure key distribution using correlated randomness in lasers driven by common random light*, Physical Review Letters, vol. **108**, 070602 (2012).

6

Scientific outcome

Publications

- Neus Oliver, Miguel C. Soriano, David W. Sukow and Ingo Fischer, *Dynamics of a semiconductor laser with polarization-rotated feedback and its utilization for random bit generation*, Optics Letters, vol. **36** No. 23, 4632-4634 (2011).

Conference Presentations

- Miguel Cornelles; Neus Oliver; Xavier Porte; Raúl Vicente; Ingo Fischer; Claudio R. Mirasso, *Delay-coupled semiconductor lasers: Dynamics and applications*. VII Reunión Iberoamericana de Óptica (RIAO) X Encuentro Latinoamericano de Óptica, Lásers y Aplicaciones, (RIAO-OPTILAS 2010). Lima (Peru), 2010. Invited talk.
- Neus Oliver, Miguel C. Soriano, David W. Sukow and Ingo Fischer, *Dynamics of semiconductor lasers with polarization rotated feedback and its applications for fast random bit generation*, European Conference on Lasers and Electro-Optics (CLEO Europe) and the XIIth European Quantum Electronics Conference 2011, Munich (Germany), 2011. Talk.
- Neus Oliver, Miguel C. Soriano, David W. Sukow and Ingo Fischer, *Dynamics of semiconductor lasers with delayed polarization-rotated feedback and its application for fast random bit generation*, Combined DPG Spring Meeting of the Section Condensed Matter and the Divisions Microprobes, Radiation and Medical Physics, Berlin (Germany), 2012. Talk.
- Neus Oliver, Miguel C. Soriano, David W. Sukow and Ingo Fischer, *Dynamics of semiconductor lasers with delayed feedback and its application for fast random bit generation*, International Conference on Delayed Complex Systems (DCS12), Palma de Mallorca (Spain), 2012. Poster.

7

Research training

Visits to other institutions

- Laser Dynamics Laboratory, National Tsing-Hua University, Hsinchu (Taiwan). Professor: Fan-Yi Lin. July - August 2011

Workshops and Summer Schools attended

- Curso de Técnicas de medida en fibras ópticas, Comité de Optoelectrónica de la SEDOPTICA, Sigüenza (Spain). 6 - 8 October 2010
- Summer School on Statistical Physics of Complex and Small Systems, IFISC, Palma de Mallorca (Spain), 12 - 23 September 2011. Oral communication: *Dynamics of semiconductor lasers subjected to polarization rotated feedback and its application for fast random bit generation.*